Hydrological and Runoff Formation Processes Based on Isotope Tracing During Ablation Period in the Source Regions of Yangtze River

Zong-Jie Li[1*], Zong-Xing Li[2*], Ling-Ling Song[3], Juan Gui[2], Jian Xue[2], Bai Juan Zhang[1], Wen De Gao[1]

[1]College of Energy and Power Engineering, Lanzhou University of Technology, Lanzhou 730050, China

[2]Observation and Research Station of Eco-Hydrology and Environmental Protection by Stable Isotope Tracing in High and Cold Mountainous Areas /Key Laboratory of Ecohydrology of Inland River Basin/Gansu Qilian Mountains Ecology Research Center, Northwest Institute of Eco-Environment and Resources, Chinese Academy of Sciences, Lanzhou 730000, China

[3]College of Forestry, Gansu Agricultural University, Lanzhou, Gansu 730070, China

*Corresponding author: Tel: 86+18993033525, E-mail: lzjie314@163.com (Zong-Jie Li), lizxhhs@163.com (Zong-Xing Li).

Abstract: This study focused on the hydrological and runoff formation processes of river water by using stable isotope tracing in the source regions of the Yangtze river during different ablation episodes in 2016 and the ablation period from 2016 to 2018. The effects of altitude on stable isotope characteristics for the river in the glacier permafrost area were greater than for the mainstream and the permafrost area during the ablation period in 2016. There was a significant negative correlation (at the 0.01 level) between precipitation and $\delta^{18}O$, while a significant positive correlation was evident between precipitation and d-excess. More interestingly, significant negative correlations appeared between $\delta^{18}O$ and temperature, relative humidity, and evaporation. A mixed segmentation model for end-members was used to determine the proportion of the contributions of different water sources to the target water body. The proportions of precipitation, supra-permafrost water, and glacier and snow meltwater for the mainstream were 41.70%, 40.88%, and 17.42%, respectively. The proportions of precipitation, supra-permafrost water, and glacier and snow meltwater were 33.63%, 42.21%, and 24.16% for the river in the glacier permafrost area and 20.79%, 69.54%, and 9.67%, respectively, for that in the permafrost area. The supra-permafrost water was relatively stable during the different ablation periods, becoming the main source of runoff in the alpine region, except for precipitation, during the ablation period.

Keywords: River water, stable isotope, ablation period, source region, Yangtze River

1. Introduction

53 Liquid precipitation, glaciers, snow, and permafrost in cold regions are important

54 components of hydrological processes, serve as a key link in the water cycle, and are

55 amplifiers and indicators of climate change (Yang et al., 2012; Chang et al., 2015; Li

56 et al., 2016a; 2016b; 2018). They are not only important as the recharge sources of

57 water in river basins but are also important resources to support regional development

58 (Halder et al., 2015; Lafrenière et al., 2019). The temporal and spatial variations of

59 runoff components are of great significance for water levels during wet and dry years

60 in terms of ecological protection and the distribution of water resources (Wang et al.,

61 2012; Pan et al., 2017; Mu et al., 2018). Therefore, the study on the composition

62 change of runoff and its hydrological effect in cold areas can not only consolidate

63 theories on runoff research, prediction, and adaptation, but also have important

64 practical significance for construction, industry, and agriculture in cold regions (Wang

65 et al., 2009; 2017; Wang et al., 2019).

66

67 The stable isotope tracer technique has become an important research method in

68 hydrology. In recent years, the response of hydrological processes to climate change

69 in cold regions has become a hot topic in the field of global change, which has greatly

70 promoted the application of the stable isotope and chemical ion tracing methods in the

71 analysis of runoff in cold regions (Li et al., 2015; 2019; Qu et al., 2017; Zhu et al.,

72 2019). Liu et al. (2004) systematically studied the contribution of glacier and snow

73 meltwater to runoff in a cold area in Colorado, USA. It was found that the

74 contribution of glacier and snow meltwater to runoff in spring was as high as 82%.

75   Boucher and Carey (2010) systematically studied runoff segmentation in permafrost

76   basins. Maurya et al. (2011) found that the average contribution of meltwater to runoff

77   was 32% in typical glacial basins on the southern slope of the Himalayas. The

78   application of the stable isotope tracer method in the analysis of runoff components in

79   the cold regions of China has been relatively small. Gu and Longinelli (1993) first

80   used $\delta^{18}O$ as a tracer in the Urumqi River in the Tianshan Mountains. The recharge

81   water source can be separated   into rainfall, snow meltwater, groundwater, and ice

82   melt water. The results showed that groundwater and snow melt water were the major

83   recharge sources of the Urumqi River in different periods and locations. Since then,

84   Kong and Pang (2012) have studied the contribution of meltwater to runoff and its

85   climatic sensitivity in two typical glacial basins in the Tianshan Mountains. The

86   composition of runoff from the Tizinafu River in the Tianshan Mountains shows that

87   the average contribution of snow melt water is 43% (Fan et al., 2015). The

88   contribution of glacier and snow meltwater to runoff in the Baishui River in the

89   Yulong Snow Mountains was 53.4% in summer (Pu et al., 2013). A study of the

90   Babao River and the Hulugou basin in the Qilian Mountains showed that different

91   water sources were fully mixed into groundwater before recharging rivers in this

92   alpine cold region, and that the contribution of meltwater in the cryosphere to runoff

93   in the cold region was as high as 33% (Li et al., 2014a; 2014b). Although these

94   studies determined the contribution of precipitation and glacier and snow meltwater to

95   runoff in the cold regions, they neglected the contribution of supra-permafrost water

96   to runoff and its impact on hydrological processes (Prasch et al., 2013; Lutz et al.,

97 2014). On the one hand, it increases the uncertainty of runoff analysis in the cold

98 regions. On the other hand, it is difficult to comprehensively evaluate the impact of

99 components on the runoff process and the hydrological effects in cold regions.

100

101 The source of the Yangtze River, which is a typical alpine frozen soil area, is an

102 important ecological barrier and a protected water source in China (Liang et al., 2008;

103 Li et al., 2017). The regional climate shows a significant warm and wet trend against

104 the background of global climate change. The regional climate shows a significant

105 warm and wet trend against the background of global climate change. So regional

106 evapotranspiration increases and ice and snow resources exhibit an accelerating

107 melting trend (Kang et al., 2007; Wang et al., 2019). The increasing of ground

108 temperature can cause it to melt significantly. The active layer becomes thicker and

109 degenerates remarkably (Shi et al., 2019). Given this background, the temporal and

110 spatial patterns, mechanisms, and influences of precipitation, glacier and snow

111 meltwater, meltwater in the active layer, and groundwater in the region undergo

112 profound changes and impact runoff processes (Wu et al., 2015). These significant

113 impacts and their hydrological effects on the entire basin have gradually become

114 prominent.

115

116 In summary, due to the lack of data and the difficulty of observation and sampling in

117 cold regions, current studies have paid more attention to the study of hydrological

118 processes and water cycle characteristics at the watershed scale from the macroscopic

119   point of view. However, there is a lack of in-depth study on the mechanism of the

120   temporal and spatial variations of runoff components from the microscopic point of

121   view, and the understanding of its hydrological effects is still in the exploratory stage.

122   At present, although stable isotope tracer techniques have been applied to the analysis

123   of runoff in cold regions, most of the current studies are limited to the assessment of

124   the contribution and impact of glacier and snow melt water but neglect the significant

125   role of liquid precipitation increase and melt water in the active layer. The results in a

126   lack of systematic understanding of the hydrological effects of runoff composition

127   changes in cold regions. Meanwhile, different types of tributaries in runoff-producing

128   areas are the key to runoff-producing processes and are the main links to

129   understanding hydrological processes in cold regions. It is urgent to develop an

130   understanding of how runoff is produced. In addition, the current study of

131   hydrological processes in the source area of the Yangtze River focuses on the

132   variation in runoff itself and its response mechanism to climate change, lacking

133   in-depth analysis of runoff components and its hydrological effects. Therefore, taking

134   the source area of the Yangtze River as an example, we conduct a study into the

135   temporal and spatial variations of isotopes in different tributary rivers under the

136   background of climate warming and their influencing factors by using the methods of

137   field observation, experimental testing, stable isotope tracing, and analytical modeling

138   of end-element mixed runoff. Based on the conversion signals of stable isotopes in

139   each link of the runoff process, at first, this study further explores the hydraulic

140   relations, recharge-drainage relations and their transformation paths, and the processes

141   of each water body. Furthermore, this study determines the composition of runoff,

142   quantifies the contribution of each runoff component to different types of tributaries.

143   Finally, this study analyzes the hydrological effects of the temporal and spatial

144   variation of runoff components. On the one hand, the research results can reveal the

145   evolution mechanism of runoff in cold regions under the background of climate

146   warming. On the other hand, it provides parameter support and a theoretical basis for

147   the simulation and prediction of runoff changes in cold regions, and then provides a

148   scientific basis for a more systematic understanding of the hydrological effects caused

149   by underlying surface changes in cold regions, ultimately providing decision-making

150   basis for the rational development and utilization of water resources in river basins.

151

152   **2. Data and Methods**

153

154   **2.1 Study area**

155

156   The source region of the Yangtze River is located in the hinterland of the Tibetan

157   Plateau (Fig. 1). It is an important ecological barrier and water conservation region in

158   China. The southern boundaries are the Tanggula Mountains and Sederi Peak, which

159   contain the watersheds of the Salween River and Lantsang River, respectively. The

160   mean altitude reaches 4000 m above sea level with a decreasing elevation from west

161   to east (Yu et al., 2013) that covers an area of approximately 138,000 km^2, 7.8% of

162   the total area of the Yangtze River Basin. Most tributaries start from glaciers, and

163   form very dense drainage networks, such as those of the Chumaer River in the north,

164   Tuotuohe River in the middle, and Dangqu River in the south (Pu, 1994). The glaciers

165 in the study area are mainly distributed along the north-oriented slopes of the

166 Tanggula Mountains and Sedir Mountains and the south-oriented slopes of the

167 Kunlun Mountains, with a total area of 1496.04 km^2 (Yao et al., 2014). The

168 permafrost has a thickness of 10 – 120 m, which accounts for 77% of the total basin

169 area, and most surface soils are frozen during winter and thaw in summer, and active

170 layer thicknesses range from 1 – 4 m (Gao et al., 2012). Annual average temperatures

171 range from 3 – 5.5°C. The annual precipitation is 221.5 – 515 mm (Yu et al., 2014).

172 The mean annual precipitation varies considerably over the reserve, and 80% of the

173 annual precipitation occurs during summer, with the highest precipitation occurring in

174 August.

175

176 **2.2 Sample Collection**

177

178 This study mainly collects precipitation, glacier and snow melt-water,

179 supra-permafrost water and river water to systematic analysis the recharge

180 relationship between precipitation, glacier and snow melt-water, supra-permafrost

181 water and river water in the source area of the Yangtze River. In this study, the initial

182 ablation period is from May to June, the strong ablation period is from July to August,

183 and the end ablation period is from September to October. In order to analyze the

184 influence of meteorological factors on the stable isotope in river water, samples were

185 collected once per week at the ZMD and TTH stations throughout the sampling period.

186 A total of 201 river water samples were collected in this study. The specific sampling

187 process is as follows:

188

River water: In order to analysis the spatial and temporal characteristic of stable

isotope of river water in mainstream (25 samples) and major tributary (including river

in glacier permafrost area (105 samples) and river in permafrost area (167 samples))

in the study area, All of river water samples around the traffic routes in the source area

of the Yangtze River were collected in initial ablation in 2016 (48 samples), ablation

in 2016 (88 samples), end ablation in 2016 (45 samples), ablation in 2017 (55 samples)

and ablation in 2018 (61 samples) (Fig.1).

196

Glacier and snow melt-water: This paper researched the hydrochemistry characteristic

of melt-water in Cryosphere (Yuzhu peak Glacier, Geladandong Glacier and

Dongkemadi Glacier) through collected water samples by fixed-point sampling from

June to September in 2016 and 2017. The samples were collected once every 10 days

at the glacier front during the ablation period. The sampling time is at 14 o'clock per

day. The sampling location is in hydrological section at the end of the glacier.

203

Supra-permafrost water: Supra-permafrost water is the most widely distributed

groundwater type in the SRYR, and it is mainly stored in the permafrost active layer

(Li et al., 2018). The hydrochemistry characteristic of supra-permafrost water in the

study area this paper collected water samples by comprehensive sampling from June

to September in 2016 and 2018. The sampling process is manual operation. At first, a

2 m deep profile of the permafrost active layer was dug at each of the sampling points.

210 Then, the collection of the water samples are immediately filtered with 0.45 um

211 Millipore filtration membrane. Then, samples were poured the filtered into a clean

212 polyethylene bottle.

213

214 Precipitation: precipitation samples were collected at Zhimenda Hydrological Station

215 (ZMD) at the mountain pass of the source area of the Yangtze River, Qumalai

216 Meteorological Station(QML) in the middle reaches of the source area and Tuotuo

217 River Meteorological Station(TTH) in the upper reaches of the source area. The

218 sampling period extended from April 1, 2016 to October 31, 2018.

219

220 Before analysis, all samples were stored at 4 ℃ in a refrigerator without evaporation.

221 Precipitation and surface water samples were analyzed for $\delta^{18}O$ and δD by means of

222 laser absorption spectroscopy (liquid water isotope analyzer, Los Gatos Research

223 DEL-100, USA) at the Key Laboratory of Ecohydrology of Inland River Basin,

224 Northwest Institute of Eco-Environment and Resources, CAS. The results are reported

225 relative to the Vienna Standard Mean Ocean Water (VSMOW). Measurement

226 precisions for $\delta^{18}O$ and δD were better than 0.5‰ and 0.2‰, respectively. Field

227 measurements included pH, dissolved oxygen (DO), electrical conductivity (EC), and

228 water temperature.

229

230 **2.3 End-Member Mixing Analysis**

231

232 Hooper (2003) introduced the end-member mixing analysis (EMMA) using

233 chemical/isotopic compositions in waters. The techniques involve graphical analyses,

234 in which chemical and isotopic parameters are used to represent the designated end

235 members. Tracer concentrations are constant in space and time. Essentially, the

236 composition of the water changing can be considered as a result of intersections

237 during its passage through each landscape zone. Tracers can be used to determine both

238 sources and flow paths. The EMMA tracer approach has been a common method for

239 analyzing potential water sources contributing to stream flow (Li et al, 2014a; 2016a).

240 Here in a three end-member mass-balance mixing model is employed to calculate the

241 contribution of up to three water sources in stream water, such as the following:

242 $$X_S = F_1 X_1 + F_2 X_2 + F_3 X_3 \quad (1a)$$

243 $$Y_S = F_1 Y_1 + F_2 Y_2 + F_3 Y_3 \quad (1b)$$

244 In Eq. (1), X and Y represent concentrations of two types of different tracers. In this

245 study, $\delta^{18}O$ and deuterium excess were chosen for comparison. The subscripts

246 represents stream water sample, and 1, 2, and 3 represent water from the respective

247 contribution of three respective source waters (end members) to stream water. The

248 fraction of each end-member is denoted by F. The solutions for F_1, F_2, and F_3 in

249 regards to tracer concentrations in Eq. (1) can be given as:

250 $$F_1 = [(X_3-X_S)/(X_3-X_2)-(Y_3-Y_S)/(Y_3-Y_2)]/[(Y_1-Y_3)/(Y_3-Y_2)-(X_1-X_3)/(X_3-X_2)] \quad (2a)$$

251 $$F_2 = [(X_3-X_S)/(X_3-X_1)-(Y_3-Y_S)/(Y_3-Y_1)]/[(Y_2-Y_3)/(Y_3-Y_1)-(X_2-X_3)/(X_3-X_1)] \quad (2b)$$

252 $$F_3 = 1 - F_1 - F_2 \quad (2c)$$

253 This method has been used by previous study (Li et al.,2014b; 2015; 2016b). This

254 study also used this method to evaluate the contribution of possible sources to the

255 river water.

256

257 **2.4 Uncertainty in hydrograph separation**

258

259   The uncertainty of tracer‑based hydrograph separations can be calculated using the

260   error propagation technique (Genereux, 1998; Klaus & McDonnell, 2013). This

261   approach considers errors of all separation equation variables. Assuming that the

262   contribution of a specific streamflow component to streamflow is a function of several

263   variables c1, c2, ⋯, cn and the uncertainty in each variable is independent of the

264   uncertainty in the others, the uncertainty in the target variable (e.g.,the contribution of

265   a specific streamflow component) is estimatedusing the following equation (Genereux,

266   1998; Uhlenbrook & Hoeg,2003):

267
$$W_{fx} = \sqrt{\left(\frac{\partial z}{\partial c_1} W_{c1}\right)^2 + \left(\frac{\partial z}{\partial c_2} W_{c2}\right)^2 + \cdots + \left(\frac{\partial z}{\partial c_n} W_{cn}\right)^2}, \qquad (3)$$

268   where W represents the uncertainty in the variable specified in the ubscript. fx is the

269   contribution of a specific streamflow component x to streamflow. The software

270   package MATLAB is used to apply equation 3 to the different hydrograph separations

271   in this study.

272

273   **3. Results**

274

275   **3.1 Temporal Variation**

276

277   As shown in Fig. 2, stable isotope characteristics of $\delta^{18}O$ and d-excess was different

278   during different ablation for the different types of runoff. For the mainstream, the $\delta^{18}O$

279   in initial ablation was higher than end ablation, while the ablation period was the

280   lowest. But $\delta^{18}O$ in ablation period showed decreasing trend from 2016 to 2018. With

281 the same as $\delta^{18}O$, d-excess in the different ablation periods was different (Fig. 2a, d).

282 For the river in the glacier permafrost area, the order of $\delta^{18}O$ for the different ablation

283 periods and the ablation period from 2016 to 2018 was the same as the mainstream

284 order, but the values of $\delta^{18}O$ were different for the mainstream (Fig. 2b, e). For the

285 river in the permafrost area, the variation $\delta^{18}O$ for the different ablation periods and

286 ablation from 2016 to 2018 was the same as for the mainstream and the river in the

287 glacier permafrost area. However, the order of d-excess was different for the river in

288 the permafrost area and the glacier permafrost area (Fig. 2c, f). In general, the $\delta^{18}O$ in

289 the mainstream was more negative than those in the rivers in the glacier permafrost

290 and permafrost areas. These results may be due to the fact that the highest runoff was

291 for the mainstream and that the effects of dilution result in lower isotope values.

292 However, the $\delta^{18}O$ in the river in the glacier permafrost area was more positive than

293 those in the mainstream and the river in the permafrost area. The effect of evaporation

294 could explain these results and the change in d-excess could also demonstrate the

295 same.

296

297 **3.2 Spatial Variation**

298

299 To analyze the spatial variation of $\delta^{18}O$ based on the different ablation periods in 2016

300 and ablation from 2016 to 2018, spatial interpolation of all river water samples in the

301 study area was performed using ArcGIS. The results are shown in Fig. 3. The $\delta^{18}O$

302 value in the north-central region of the study area was more positive than those in

303 other regions. In the southeastern part of the study area, especially the QML, ZMD,

304 and Tanggula Mountains, the values were more negative during the initial ablation

305 period. The area of positive ablation during the ablation period, which was

306 concentrated mainly in the northeast part of the study area, was larger than that during

307 the initial ablation. The other regions, except some areas in the southwest, turned

308 positive. The area of positive ablation was largest during the final of the different

309 ablation periods in 2016; all areas, except some in the eastern region of the study area,

310 were positive (Fig. 3). The area of positive ablation in the central and northern regions

311 began to expand in 2017 compared to the area of ablation in 2016. Furthermore, the

312 area of negative ablation appears mainly in the southeastern and southwestern

313 portions of the study area. However, the positive ablation area was also concentrated

314 in the central and northern regions in 2018 and it was greater than it was in 2016 and

315 2017. Meanwhile, the negative ablation area appeared mainly in the southeastern and

316 southwestern portions of the study area, but it was smaller than in 2016 and 2017.

317 These results may be related to evaporation, possible recharge sources, or

318 meteorological factors. These results were comprehensive and influenced by

319 meteorological factors and the type and proportion of recharge sources. The

320 evaporation effect was strong in the central and northern regions, which were also the

321 major glacier and permafrost regions. The southeastern region was the downstream

322 area where all runoff converged; thus, the dilution effect led to a more negative $\delta^{18}O$

323 here. Moreover, the Tanggula Mountains, with altitudes higher than those in other

324 regions, were located southwest of the study area; thus, evaporation had a low

325 influence on this region and the oxygen stable isotopes were more negative.

326

327   Just as with the spatial distribution of $\delta^{18}O$, there was a significant spatial distribution

328   of d-excess in the study area (Fig. 4). Compared to the spatial distribution of $\delta^{18}O$, the

329   d-excess in the central and northern regions were lower than those in the other regions.

330   However, d-excess was higher in the latter, especially in the southwestern regions and

331   in the southeastern regions during the initial ablation period. The lower area begin to

332   expand during the ablation period in 2016, while the central and northeastern regions

333   and the Tanggula Mountains were greater. Meanwhile, the negative ablation area

334   continued to expand during the end ablation period; ablation was greater only in the

335   southeastern part of the study area. However, all regions except for areas in the

336   eastern region where the ablation was low during the ablation period in 2017

337   exhibited high ablation especially Tanggula Mountains. Moreover, the lower ablation

338   regions appeared mainly in the central and southeastern regions of the study area;

339   values were higher in the other regions, especially in the Tanggula Mountains and the

340   northeast. The spatial distribution of d-excess also confirmed the spatial distribution

341   of the oxygen stable isotope because evaporation resulted in the enrichment of

342   isotopes and led to a reduction in d-excess.

343

344   In general, the influence of evaporation on the isotope and d-excess was only

345   manifested in some places, such as the central and northern parts of the study area, in

346   the initial ablation and the   ablation periods. However, the influence of evaporation

347   on the isotope and d-excess was manifested in most places, except the southeast of the

348   study area. Meanwhile, these results also indicated that there may be a hysteresis for

349   the influence of meteorological factors on isotopes and d-excess. On the one hand,

350   river water was the result of the final convergence of various recharge sources that

351   include precipitation, supra-permafrost water, and glacier and snow meltwater. On the

352   other hand, meteorological factors directly affected the main recharge sources of river

353   water.

354

355   As shown in Fig. 5, there was a significant difference in the variation of $\delta^{18}O$ and

356   d-excess with altitude for the mainstream, the river in the glacier permafrost area, and

357   the river in the permafrost area of the study area. For the mainstream, the oxygen

358   stable isotope showed a decreasing trend, with increases in altitude, during the

359   ablation periods in 2016 and 2018. In other words, the altitude effect only appeared in

360   the ablation periods during these two years and had values of −0.16‰/100 m

361   ($p < 0.05$) and −0.14‰/100 m ($p < 0.05$), respectively. However, $\delta^{18}O$ showed an

362   increasing trend with an increase in altitude during the initial and end ablation periods

363   in 2016 and   ablation period in 2017. The anti-altitude effects of the initial and end

364   ablation periods in 2016, and   ablation period in 2017, were 0.11‰/100 m ($p < 0.05$),

365   0.13‰/100 m ($p < 0.01$), and 0.04‰/100 m ($p < 0.05$), respectively. For the

366   phenomenon of anti-altitude effect, the following reasons can explain this

367   phenomenon: on the one hand, in the source area of the river, the stable isotope

368   concentration of precipitation and glacier snow meltwater is relatively low and the

369   value of groundwater in the permafrost active layer is relatively positive due to the

370   influence of soil evaporation; On the other hand, the more the inflow of precipitation,

371   the greater the contribution of precipitation. So there is an obvious diluting effect of

372   biotin, which makes the concentration more negative. D-excess showed a decreasing

373   trend during the initial and end ablation periods in 2016 and a significant increasing

374   trend in the   ablation period from 2016 to 2018. For the river in the glacier

375   permafrost area, $\delta^{18}O$ showed a decreasing trend with increase in altitude during the

376   ablation periods in 2016 and 2018, but the ablation in 2018 was not significant. The

377   altitude effect was $-0.66‰/100$ m ($p < 0.05$) and $-0.15‰/100$ m ($p > 0.05$),

378   respectively, during the former two periods. Moreover, a significant anti-altitude

379   effect of $0.47‰/100$ m ($p < 0.05$), $0.67‰/100$ m ($p < 0.05$), and $0.97‰/100$ m

380   ($p < 0.05$), appeared in the initial and end ablation periods in 2016 and   ablation

381   period in 2017, respectively. Just as with the mainstream, d-excess showed a

382   decreasing trend in the initial and end ablation periods in 2016 and an increasing trend

383   in the   ablation from 2016 to 2018. For the river in the permafrost area, $\delta^{18}O$ showed

384   a decreasing trend with an increase in altitude in the initial ablation period and

385   ablation period in 2016, with an altitude effect of $-0.38‰/100$ m ($p < 0.05$) and

386    $-0.12‰/100$ m ($p > 0.05$), respectively. However, $\delta^{18}O$ showed an increasing trend

387   with increase in altitude in the end ablation period in 2016 and the   ablation periods

388   in 2017 and 2018, with an anti-altitude effect of $0.21‰/100$ m ($p < 0.05$),

389    $0.01‰/100$ m ($p > 0.05$), and $0.68‰/100$ m ($p < 0.05$), respectively. d-excess showed

390   an increasing trend with increase in altitude in the initial and end ablation periods in

391   2016 and   ablation periods in 2016 and 2017. However, d-excess also showed a

392   decreasing trend with increase in altitude in the ablation period in 2018.

393

394   In summary, the altitude effect mainly appeared during ablation, whether it was in the

395   mainstream, the river in the glacier permafrost area, or the river in the permafrost area.

396   The altitude effects were higher for the river in the glacier permafrost area than for the

397   mainstream or the river in the permafrost area during the ablation period in 2016.

398   Meanwhile, the anti-altitude effect of the river in the glacier permafrost area was

399   higher than that of the other areas. The $\delta^{18}O$ during the initial and end ablation periods

400   in 2016 showed a significant anti-altitude effect for the mainstream and the river in

401   the glacier permafrost area; a significant altitude effect appeared during the initial

402   ablation period for the river in the permafrost area. These results may be due to the

403   comprehensive influence of possible recharge sources and different recharge

404   proportions caused by the influence of meteorological factors. This kind of

405   comprehensive influence is mainly due to the significant seasonality of climate factors

406   in the cold regions, which directly determines the types and contribution proportion of

407   possible recharge sources. Therefore, this result can not be said to be caused by any

408   one factor, but can only be explained by the comprehensive influence of possible

409   recharge sources and different recharge proportions caused by the influence of

410   meteorological factors.

411

412   **3.3 Evaporation Line**

413

414   The variations in the location of the evaporation line for river water during the

different ablation periods in 2016 and the ablation periods from 2016 to 2018 are

shown in Fig. 6. The slope and intercept of the LEL for river water showed an

increasing trend from the initial to end ablation periods in 2016. The LEL in the initial

ablation period was $\delta D = 6.59\delta^{18}O - 3.60$ (p < 0.01) and it was $\delta D = 6.88\delta^{18}O - 1.37$

(p < 0.01) during the ablation period. The LEL during the end ablation period was

$\delta D = 7.39\delta^{18}O + 5.88$ (p < 0.01). These results indicate that the effect of evaporation

on the stable isotopes in river water gradually weakened from the initial ablation to

the end ablation periods. The slope and intercept of the LEL of river water during the

ablation period in 2017 were lower than those in 2016. The LEL during the ablation

period in 2017 was $\delta D = 6.59\delta^{18}O - 3.63$ (p < 0.01). However, whether the slope or

the intercept of LEL of river water in 2018 was higher than that in 2016 and 2017,

with the LEL was: $\delta D = 7.63\delta^{18}O + 5.82$ (p < 0.01). This phenomenon showed that

the influence of evaporation on stable isotope levels was greatest during the ablation

period in 2017, followed by that in 2016. In general, the lower slope and intercept

indicate that the water body was affected by evaporation or non-equilibrium dynamic

fractionation. This conclusion could also explain the results of this study.

3.4 Recharge Sources

The distribution of δD and $\delta^{18}O$ for river water among other water bodies are shown

in Fig. 7 during the different ablation periods in 2016 and ablation from 2016 to 2018.

The results of the distribution of δD and $\delta^{18}O$ of river water indicate the possible

recharge sources of river water. However, the δD and $\delta^{18}O$ of river water,

438   supra-permafrost water, glacier snow meltwater, and precipitation exhibited little

439   change during the initial ablation in 2016 (Fig. 7a, b). This phenomenon suggests that

440   precipitation may be the major recharge sources for river water during the initial

441   ablation. A plot of δD versus $\delta^{18}O$ for river and supra-permafrost water, glacier snow

442   meltwater, and precipitation is shown in Fig. 7c. The δD and $\delta^{18}O$ values of glacier

443   and snow meltwater from above the LMWL are the most negative compared to other

444   water bodies. The stable isotope of supra-permafrost water was relatively more

445   positive, located below the LMWL, confirming the influence of strong evaporation.

446   The stable isotope of river water was close to the LMWL, and its concentration value

447   was between precipitation, glacier and snow meltwater, and supra-permafrost water,

448   reflecting that river water was recharged and affected by multi-source water in the

449   study area. Moreover, the distribution of river water, glacier and snow meltwater, and

450   supra-permafrost water also indicated that there was a hydraulic relationship between

451   the source and target in the different ablation periods in 2016 and ablation from 2016

452   to 2018.

453

454   The mixed segmentation model of the end-member is used to determine the

455   contribution proportions of different water sources to the target water. Owing to the

456   two stable isotope concentrations in different water bodies have significant spatial and

457   temporal differences, it can effectively distinguish different water bodies and their

458   mixing relationships. The d-excess and $\delta^{18}O$ are used as tracers of the mixed

459   segmentation model of the end-elements. As shown in Fig. 8, according to the

460   locations of the different types of water and the distance from other water bodies,

461   which reflected the mixed recharge of three water bodies, supra-permafrost water was

462   the first end element, precipitation was the second end element, and glacier and snow

463   meltwater was the third end element. However, the different runoffs likely have

464   different recharge sources and different recharge proportions. The glacier permafrost

465   area river comprised glacier and snow meltwater more in the ablation period than in

466   other periods. Compared with the permafrost area river and the glacier permafrost

467   area river, the mainstream was governed by the supra-permafrost water in the initial

468   ablation period while containing nearly equal proportions of supra-permafrost water

469   and precipitation in the end ablation period. However, the mainstream received

470   significant contributions from all three end members in the ablation period from 2016

471   to 2018 and particularly in 2017.

472

473   The recharge proportions of precipitation, supra-permafrost water, and glacier and

474   snow meltwater at different altitudes are depicted in Fig. 9, from the mixed

475   segmentation model of the three end-members during the ablation periods mentioned

476   above. The recharge proportions of the three end members in the ablation periods

477   were significantly different. This may be due to the different effects of the runoff

478   recharge sources in different ablation periods, as well as the significant differences in

479   recharge and drainage relationships in the different ablation periods. The recharge

480   proportions of precipitation in the initial ablation in 2016, ablation in 2016, end

481   ablation in 2016, ablation in 2017, and ablation in 2018, obtained by calculating the

average contribution proportion from each altitude, were 28.71%, 44.41%, 44.60%, 42.53%, and 51.03%, respectively. Meanwhile, the recharge proportions of supra-permafrost water in the initial ablation in 2016, ablation in 2016, end ablation in 2016, ablation in 2017, and ablation in 2018 were 55.38%, 36.51%, 40.21%, 37.56%, and 28.87%, respectively. The recharge proportions of glacier and snow meltwater in the initial ablation in 2016, ablation in 2016, end ablation in 2016, ablation in 2017, and ablation in 2018 were 15.91%, 19.08%, 15.19%, 19.90%, and 20.09%, respectively. The recharge proportion of precipitation decreased with increase in altitude in the initial ablation, while the proportion of supra-permafrost water and glacier and snow meltwater exhibited an increasing trend with increase in altitude. However, the recharge proportion of the supra-permafrost water was higher than that of precipitation or glacier and snow meltwater, and also showed a decreasing trend from low to high altitude in the end ablation in 2016. The proportion of glacier and snow meltwater increased with increase in altitude, but the recharge proportion of supra-permafrost water was stable with the change in altitude in the end ablation in 2016. The trend of precipitation and glacier and snow meltwater for the ablation was the same as that for the initial and end ablation. However, the recharge proportion of precipitation was higher than the proportion of supra-permafrost water and glacier and snow meltwater in the ablation period. Meanwhile, the recharge proportion of glacier and snow meltwater in ablation was higher than that in the initial and end ablation period. In general, the recharge of supra-permafrost water to runoff was stable, whether in the different ablation periods in 2016 or the ablation from 2016 to 2018.

504   However, the proportion of supra-permafrost water was relatively low, mainly due to

505   the larger runoff during the ablation period.

506

507   Using the approach shown in Equation (3), the uncertainty originating from the

508   variation in the tracers of components and measurement methods could be calculated

509   separately (Uhlenbrook & Hoeg, 2003; Pu et al., 2013). According to the calculations

510   made using Equation (3), the uncertainty was estimated to be 0.07 for the three‑

511   component mixing model in the study region. The uncertainty terms for

512   supra-permafrost water accounted for more than 50.0% of the total uncertainty,

513   indicating that the $\delta^{18}O$ and δD variations of supra-permafrost water accounted for the

514   majority of the uncertainty. Although there is some uncertainty for hydrograph

515   separation, isotope-based hydrograph separations are still valuable tools for evaluating

516   the contribution of meltwater to water resources, and they are particularly helpful for

517   improving our understanding of hydrological processes in cold regions, where there is

518   a lack of observational data.

519

520   **4. Discussions**

521

522   **4.1 Meteorological Factors**

523

524   To further explain the reason for the variation in temporal and spatial characteristics

525   of stable isotopes and LEL, this study includes the analysis of the monthly change in

526   precipitation, temperature, relative humidity, and evaporation during the sampling

527   period (from January 2016 to December 2018). The results are shown in Fig. 10. The

528   average of the precipitation was 371.9 mm during the sampling period, and the

529   precipitation in the   ablation period accounted for 78.87%. The average of the

530   temperature, relative humidity, and evaporation during the sampling period were

531   −1.42 °C, 52.20%, and 4.14 mm, respectively. However, the average of the

532   temperature, relative humidity, and evaporation during the ablation period were

533   8.04 °C, 66.47%, and 5.57 mm, respectively.

534

535   More importantly, the precipitation during the initial, total, and end ablation periods in

536   2016, and the   ablation periods in 2017 and 2018, were 50.40 mm, 107.90 mm,

537   42.90 mm, 70.60 mm, and 119.00 mm, respectively. For precipitation, the isotope

538   levels tend to decrease with the increase in rainfall; Precipitation is also the major

539   source of water for all water bodies (Maurya et al., 2011; Pu et al., 2013; Li et al.,

540   2014b; 2015; 2016a; 2018; Pan et al., 2017) and, in general, more precipitation

541   resulted in a greater dilution effect. A more negative $\delta^{18}O$ appeared in the ablation

542   period in 2016 whether in all three study areas given the change in $\delta^{18}O$ (Fig. 2). This

543   result showed that dilution does not only play an important role in the precipitation

544   effect; it also affects river water. However, the dilution effect was also significant

545   when precipitation was the major recharge source for river water (Abongwa and

546   Atekwana, 2018; Li et al., 2015).

547

548   Temperature for the initial, total, and end ablation periods in 2016, and the ablation

549   periods in 2017 and 2018, were 6.82 °C, 9.58 °C, 3.77 °C, 9.47 °C, and 11.09 °C,

550 respectively. For atmospheric precipitation, the lower the temperature was, the higher

551 the condensation degree of water vapor exhibited and the lower the isotope content in

552 precipitation. Therefore, there is a positive correlation between the stable isotope and

553 temperature in precipitation (Li et al., 2016a). However, the influence of temperature

554 on the stable isotope of river water was not significant from the variation in river

555 water isotope during the different ablation periods. However, the variation trend of the

556 stable isotope of river water in the ablation period from 2016 to 2018 was similar to

557 that for the change in temperature. Meanwhile, the variation trend of d-excess can

558 also be confirmed by this analysis (Fig. 2).

559

560 Relative humidity in the initial ablation, ablation, and end ablation periods in 2016

561 and the ablation periods in 2017 and 2018 were 60.07%, 63.16%, 70.57%, 63.39%,

562 and 63.48%, respectively. When the relative humidity is low, the dynamic

563 fractionation increases and the slope decreases, and vice versa. The variation trend of

564 the slope of the LEL for the different ablation periods in 2016 was the same as that for

565 the change in relative humidity (Fig. 6). Meanwhile, the intercept of the LEL for the

566 different ablation periods in 2016 also showed the same trend.

567

568 Evaporation in the initial ablation, ablation, and end ablation periods in 2016 and

569 ablation periods in 2017 and 2018 were 6.69 mm, 6.96 mm, 4.02 mm, 6.48 mm, and

570 6.02 mm, respectively. The stable isotopes of hydrogen and oxygen in river water are

571 comprehensively affected by the evaporation process, runoff change, precipitation

recharge, glacier and snow meltwater recharge and supra-permafrost water in cold regions. During the process of evaporation, lighter water isotopes are separated preferentially from the surface of water while heavier isotopes are enriched in the remaining water body. Evaporation enriches the oxygen and hydrogen stable isotopes and reduces excess deuterium (Li et al., 2015; 2018). The trend in the oxygen isotope in the   ablation periods from 2016 to 2018 was the same as that for the change in evaporation (Fig. 2). Meanwhile, the spatial distribution of $\delta^{18}O$ and d-excess also responded to this change (Fig. 3, 4).

To further analyze the influence of meteorological factors on the stable isotope, the correlation analysis between meteorological factors and the monthly value of $\delta^{18}O$ and d-excess, which showed continuous observations at two fixed-point stations was analyzed (Table 1), and the results are shown in Table 1. There was a significant negative correlation between precipitation and $\delta^{18}O$ at the 0.01 level (2-tailed), while a significant positive correlation between precipitation and d-excess was also present. More interestingly, just as with precipitation, a significant negative correlation appeared between $\delta^{18}O$ and temperature, relative humidity, and evaporation, with coefficients of -0.671, -0.555, and -0.636, respectively. Meanwhile, a significant positive correlation occurred between d-excess and temperature, relative humidity, and evaporation, with coefficients of 0.602, 0.524, and 0.533, respectively. This results indicated that the direct influence of meteorological factors on stable isotopes of river water was significant and definite.

594

Hydrogen and oxygen isotope compositions in river water are the result of the combined effects of the isotopes making up present in precipitation, glacier and snow meltwater, and supra-permafrost water as well as evaporative fractionation (Li et al., 2015). The main influential hydrometeorological factors include precipitation, temperature, relative humidity, and evaporation. On the whole, river water isotopes were not influenced by a single factor; instead, they were based on the comprehensive influence of many factors in the cold regions. The influence of meteorological factors on different types of river water (mainstream, rivers in glacier permafrost areas, and rivers in permafrost areas) showed that apart from their directly influences, each factor indirectly affected the river water recharge source. This indirect influence was mainly felt on precipitation, glacier, snow, and permafrost.

606

607

4.2 Hydrological processes

609

To systematically quantify the main recharge sources of different types of runoff in the alpine regions, the possible sources and recharge proportions of runoff of different types in different ablation periods were deeply analyzed by using the mixed segmentation model of the three end-members in this study. The conceptual model map of the recharge form and proportion of the river water in the different ablation periods is shown in Fig. 11.

616

617   For the river in the glacier permafrost area, there was a significant difference in the

618   recharge proportion in the runoff area, in which there were several glaciers and

619   permafrost in the basin, and other areas during the various ablation periods. The

620   proportion of recharge from precipitation during the initial, total, and end ablations in

621   2016, the   ablation in 2017, and the   ablation in 2018 were 27.69%, 33.71%,

622   32.38%, 33.21%, and 41.48%, respectively. However, the proportion of

623   supra-permafrost water in the initial, total, and end ablations in 2016, the   ablation in

624   2017, and the   ablation in 2018 were 54.68%, 35.96%, 46.38%, 37.39%, and 36.63%,

625   respectively. The proportions of glacier and snow meltwater in the initial, total, and

626   end ablations in 2016, the   ablation in 2017, and the   ablation in 2018 were 17.63%,

627   30.33%, 21.24%, 29.39%, and 22.19%, respectively. These results show that

628   supra-permafrost water was the important recharge source for runoff during the initial

629   and end ablation periods. The proportion of supra-permafrost water was 50.53%

630   during the initial and end ablation periods. It was also the next highest source of

631   runoff recharge, next to precipitation, during the ablation from 2016 to 2018; the

632   proportions were 36.13% and 36.66%, respectively. The recharge proportions for

633   glacier and snow meltwater was higher during the ablation period than in the initial

634   and end ablation periods, at 19.44% and 27.30%, respectively.

635

636   For permafrost area river, the runoff area only with permafrost and no glacier in the

637   basin, there was also an obvious difference for the recharge proportion in different

638   ablation period. Compared with the glacier permafrost area river the recharge

639   proportion of supra-permafrost water was higher for permafrost area river than that

640   for the glacier permafrost area river (42.21%). The recharge proportion of

641   supra-permafrost water was 69.54%. With the same as the glacier permafrost area

642   river, the supra-permafrost water was the important recharge sources to runoff in the

643   initial and end ablation, and the proportion was 80.97% in the initial and end ablation

644   period. Meanwhile, the proportion of supra-permafrost water was 61.92% in the

645   ablation period. The proportion was higher than that for precipitation (24.13%) in the

646   ablation period. In general, the supra-permafrost water was the major recharge source

647   for the permafrost area river in the different ablation periods in the study area.

648   Meanwhile, the glacier and snow meltwater had little contribution to the permafrost

649   area river in the initial and end ablation periods.

650

651   For the mainstream, the recharge proportions for precipitation during the initial, total,

652   and end ablations in 2016, the ablation in 2017, and the ablation in 2018 were 28.67%,

653   48.35%, 43.18%, 46.97%, and 41.33%, respectively. The proportion was 35.93% in

654   the initial and end ablation periods and 45.55% in the ablation period. However, the

655   proportions of supra-permafrost water during the initial, total, and end ablation in

656   2016, the ablation in 2017, and the ablation in 2018 were 52.37%, 33.52%, 42.61%,

657   39.68%, and 38.21%, respectively. The proportion was 47.49% during the initial and

658   end ablation periods and 36.47% during the ablation period. These results indicate

659   that, for the study area, the supra-permafrost water was the major recharge source for

660   the mainstream in the first two of these ablation periods while precipitation was the

661   major recharge source for the mainstream in the ablation period. The proportions of

662   glacier and snow meltwater during the initial, total, and end ablation in 2016, the

663   ablation in 2017, and the ablation in 2018 were 18.96%, 20.13%, 14.21%, 13.35%,

664   and 20.46%, respectively. The proportion of glacier and snow meltwater for the

665   mainstream (16.59%) was higher than that for the river in the permafrost area (3.25%)

666   but lower than that for the river in the glacier permafrost area (19.44%) during the

667   initial and end ablation periods. The former proportion was also higher than that for

668   the river in the permafrost area (17.98% vs 13.95%) but lower than that for the river

669   in the glacier permafrost area (27.30%) during the ablation period.

670

671   The hydrological process in cold regions has one particularity. The low permeability

672   in permafrost layer and the freeze-thaw depths of the soil reduces soil infiltration (Wu

673   et al., 2015; Wang et al., 2019). Therefore, the rapid replenishment of meltwater by

674   runoff results in a difference in the runoff generation mechanism in the permafrost

675   and non-permafrost regions (Yang et al., 2010; Li et al., 2018). Moreover, because the

676   freeze-thaw depths of the soil changes with annual fluctuations in temperature, there

677   is an effect on soil water storage capacity that results in a difference in the runoff

678   generation mechanism during different ablation periods (Wang et al., 2019). Wang et

679   al. (2008) also found that the seasonal distributions and variations in rainfall runoff in

680   the permafrost basin were controlled by the freeze-thaw process because of the

681   impermeable nature of the freeze-thaw front and permafrost layer. During the initial

682   ablation period, the supra-permafrost water—whether in the mainstream, the river in

683   the glacier permafrost area, or the river in the permafrost area—was the major

684   recharge source. During the ablation period, precipitation was the main source of

685   runoff recharge, followed by supra-permafrost water. Although there was little

686   difference the proportion of precipitation and supra-permafrost water during the

687   ablations from 2016 to 2018, precipitation was the major recharge source of runoff in

688   this period. Supra-permafrost water was the main source of runoff recharge in the end

689   ablation period, just as it was in the initial ablation period. In summary, runoff in the

690   cold region during the different ablation periods was mainly composed of runoff from

691   rainfall, meltwater, and supra-permafrost. Because of the inherent seasonal variation

692   in precipitation, there were significant changes in precipitation during the different

693   ablation periods. Glacier and snow meltwater was also greatly affected by climatic

694   factors during the different ablation periods, while the supra-permafrost water was

695   relatively stable; the latter became the main source of runoff supply, except for

696   precipitation, in the alpine region. Thus, with the changes that the low temperatures

697   made in the physical properties of the underlying surface, the change in the

698   permafrost had the most significant effect on the hydrological process in cold regions.

699

700   **4.3 Hydrological significance of permafrost**

701

702   The source region of the Yangtze River is a typical permafrost area. The permafrost

703   area is 107619.13 km^2, which accounting for 77% of the total area. The seasonal

704   frozen soil is mainly distributed in the valley area, with an area of 30754.34 km^2.

705   Field observation and research confirmed that most of the precipitation in permafrost

area is frozen on the ground or used to recharge the deficit of soil water, and does not directly form runoff in permafrost area. Under the background of permafrost degradation, the area of permafrost is gradually shrinking and the thickness of permafrost is gradually decreasing with the increase of the thickness of active layer. The degradation of ice rich permafrost in the cold regions has an important contribution to the development of surface runoff and hot karst lakes. Due to the decrease of permafrost water storage capacity in the Qinghai Tibet Plateau, the availability of water resources will be reduced in dry season, and the increase of water melting may lead to the increase of flood risk, and the resilience of ecosystem will be reduced through the seasonal changes of river flow and groundwater abundance. All these changes will affect the water resources balance and sustainable development of the Qinghai Tibet Plateau, including the headwaters of major rivers in Asia, including the Yellow River, the Yangtze River, the Salween River, the Mekong River, the Brahmaputra River, the Ganges River, the Indus River, the Ili River, the Tarim River, the Erqis River and the Yenisei River Rivers, these rivers provide fresh water resources for the survival of about 2 billion people.

In brief, the freeze-thaw of soil in the active layer plays an important role in controlling river runoff. The increase in melting depth leads to a decrease in the direct runoff rate and slow dewatering process. The two processes of runoff retreat are the result of soil freeze-thaw in the active layer. Permafrost has two hydrological functions: on the one hand, permafrost is an impervious layer, and it has the function

of preventing surface water or liquid water from infiltrating into deep soil; on the

other hand, it forms a soil temperature gradient, which makes the soil moisture close

to the ice cover. Therefore, changes in the soil water capacity, soil water permeability,

and soil water conductivity, as well as the redistribution of water in the soil profile,

are caused by the freeze-thaw of the active layer. The seasonal freeze-thaw process of

the active layer directly leads to seasonal flow changes in surface water and

groundwater, which affects surface runoff. Climate warming is the main driving force

in the degradation of cold ecosystems (Wang et al., 2009; Wu et al., 2015; Li et al.,

2018; Wang et al., 2019). More importantly, under the background of intense melting,

the melting water of the cryosphere has had a significant impact on the hydrological

process in the cold region. The hydrological function of groundwater in the

permafrost active layer should be paid more attention, especially in the cold region

where glaciers are about to subside, its hydrological function needs to be recognized.

The stable isotope characteristics of the cryosphere are more complex than other

regions, and its mechanism is more complex further research is needed.

5. Conclusions

Through systematically analysis of the characteristics of $\delta^{18}O$, δD, and d-excess of

river water in the different ablation periods in 2016 and the ablation periods from2016

to 2018, the results were as follows. The temporal and spatial characteristics of stable

isotopes of river water were significant in the study area. The $\delta^{18}O$ in mainstream was

more negative than that in the glacier permafrost area river and permafrost area river.

751   The influence of evaporation on isotope and d-excess is only prevalent in some places,

752   such as the central and northern parts of the study area in the initial ablation and

753   ablation periods. However, the influence of evaporation on isotope and d-excess is

754   prevalent in most places except the southeastern part of the study area. Meanwhile,

755   this results also indicated that there may be a hysteresis for the influence of

756   meteorological factors on isotopes and d-excess. The altitude effect is only present

757   during the ablation periods in 2016 and 2018, and the altitude effect was −0.16‰/100

758   m (p < 0.05) and −0.14‰/100 m (p < 0.05). The slope of LEL for river water showed

759   an increasing trend from initial ablation to end ablation in 2016. Meanwhile, the

760   intercept of LEL for river water also increased from the initial ablation to the end

761   ablation period. Moreover, the mixed segmentation model of the end-member is used

762   to determine the contribution proportion of different water sources to the target water.

763   The results showed that the supra-permafrost water was the major recharge source for

764   the permafrost area river in the study area. Meanwhile, the glacier and snow

765   meltwater contributed little to the permafrost area river in the initial and end ablation

766   periods. For the mainstream, the proportion was 35.93% in initial and end ablation

767   periods, and 45.55% in the   ablation period. However, the proportion was 47.49% in

768   the initial and end ablation periods, and 36.47% in the ablation period. The proportion

769   of glacier and snow meltwater for the mainstream (16.59%) was higher than that for

770   the permafrost area river (3.25%) but was lower than that for the glacier permafrost

771   area river (19.44%) in the initial and end ablation periods. Meanwhile, the proportion

772   of glacier and snow meltwater for the mainstream (17.98%) was higher than that for

the permafrost area river (13.95%) but was lower than that for the glacier permafrost

area river (27.30%) in the ablation period.

Data availability

The data that support the findings of this study are available from the corresponding

author upon reasonable request.

Author contributions

1. ZongJie Li: Writing - Original Draft;Methodology;Formal analysis; 2.ZongXing Li:Writing - Review & Editing;Conceptualization;Resources;Supervision;Project administration; 3.LingLing Song: Software;Validation;Data Curation; 4.Juan Gui:Investigation;Data Curation; 5.Jian Xue:Investigation;Formal analysis; 6.BaiJuan Zhang:Investigation;Data Curation; 7.WenDe Gao:Data Curation.

Competing interests

The authors declare that they have no conflict of interest.

Acknowledges

803

804 **References**

805

806 Abongwa, P. T., & Atekwana, E. A. : A laboratory study investigating the effects of

807 dilution by precipitation on dissolved inorganic carbon and stable isotope

808 evolution in surface waters. Environ Sci Pollu Res, 25(20), 19941-19952.

809 https://doi.org/10.1007/s11356-018-2085-0, 2018.

810 Banner, J. L., & Hanson, G. N. : Calculation of simultaneous isotopic and trace

811 element variations during water-rock interaction with applications to carbonate

812 diagenesis. Geochim Cosmochim Ac, 54(11), 3123-3137.

813 https://doi.org/10.1016/0016-7037(90)90128-8, 1990.

814 Boucher, J. L., & Carey, S. K.: Exploring runoff processes using chemical, isotopic

815 and hydrometric data in a discontinuous permafrost catchment. Hydro Res, 41(6),

816 508-519. https://doi.org/10.2166/nh.2010.146, 2010.

817 Chang, J., Wang, G., & Mao, T. : Simulation and prediction of suprapermafrost

818 groundwater level variation in response to climate change using a neural network

819 model. J Hydro, 529, 1211-1220. https://doi.org/10.1016/j.jhydrol.2015.09.038,

820   2015.

821   Fan, Y., Chen, Y., Li, X., Li, W., & Li, Q. : Characteristics of water isotopes and

822   ice-snowmelt quantification in the Tizinafu River, north Kunlun Mountains,

823   Central   Asia.   Quater   inter,   380,   116-122.

824   https://doi.org/10.1016/j.quaint.2014.05.020, 2015.

825   Halder, J., Terzer, S., Wassenaar, L. I., Araguás-Araguás, L. J., & Aggarwal, P. K. :

826   The Global Network of Isotopes in Rivers (GNIR): integration of water isotopes

827   in watershed observation and riverine research. Hydrol Earth Sys Sc, 19(8),

828   3419-3431. https://doi.org/10.5194/hess-19-3419-2015, 2015.

829   Hooper, R. P. : Diagnostic tools for mixing models of stream water chemistry. Water

830   Resour Res, 39(3): 1055. https://doi.org/10.1029/2002WR001528, 2003.

831   Horita, J., Driesner, T., & Cole, D. R. : Hydrogen isotope fractionation in the system

832   brucite-water±NaCl to elevated temperatures and pressures: Implications for the

833   isotopic property of NaCl fluids under geologic conditions. Geochim

834   Cosmochim Aca, 235, 140-152. https://doi.org/10.1016/j.gca.2018.05.031, 2018.

835   Gao, H., He, X., Ye, B., & Pu, J. : Modeling the runoff and glacier mass balance in a

836   small watershed on the Central Tibetan Plateau, China, from 1955 to 2008.

837   Hydro Pro, 26(11), 1593-1603. https://doi.org/10.1002/hyp.8256, 2012.

838   Genereux, D. : Quantifying uncertainty in tracer‐based hydrograph separations.

839   Water Resour Res, 34(4), 915-919.   https://doi.org/10.1029/98WR00010, 1998.

840   Gu, W. Z., & Longinelli, A. : A case study on the hydrological significance of stable

841   isotope data on alpine catchments with snow cover and glaciers, Xinjiang, China.

842   IAHS Publications-Publications of the Inter Asso Hydro Sci, 218, 371-384,

843   1993.

844   Jin, H., Zhao, L., Wang, S., & Jin, R. : Thermal regimes and degradation modes of

845   permafrost along the Qinghai-Tibet Highway. Sci China Ser D: Earth Sci, 49(11),

846   1170-1183. https://doi.org/10.1007/s11430-006-2003-z, 2006.

847   Kang, S., Zhang, Y., Qin, D., Ren, J., Zhang, Q., Grigholm, B., & Mayewski, P. A. :

848   Recent temperature increase recorded in an ice core in the source region of

849   Yangtze   River.   Chinese   Sci   Bull,   52(6),   825-831.

850   https://doi.org/10.1007/s11434-007-0140-1, 2007.

851   Klaus, J., & McDonnell, J. J. : Hydrograph separation using stable isotopes: Review

852   and   evaluation.   J   Hydro,   505,   47-64.

853   https://doi.org/10.1016/j.jhydrol.2013.09.006, 2013.

854   Kong, Y., & Pang, Z. : Evaluating the sensitivity of glacier rivers to climate change

855   based on hydrograph separation of discharge. J Hydro, 434, 121-129.

856   https://doi.org/10.1016/j.jhydrol.2012.02.029, 2012.

857   Lafrenière, M. J., & Lamoureux, S. F. : Effects of changing permafrost conditions on

858   hydrological processes and fluvial fluxes. Earth-Sci Rev, 191,212-223.

859   https://doi.org/10.1016/j.earscirev.2019.02.018, 2019.

860   Li, C., Yang, S., Lian, E., Yang, C., Deng, K., & Liu, Z. : Damming effect on the

861   Changjiang (Yangtze River) river water cycle based on stable hydrogen and

862   oxygen   isotopic   records.   J   Geochem   Explor,   165,   125-133.

863   https://doi.org/10.1016/j.gexplo.2016.03.006, 2016.

Li, Z.X., Qi, F., Wei, L., Tingting, W., Aifang, C., Yan, G., ... & Bing, J. : Study on the contribution of cryosphere to runoff in the cold alpine basin: A case study of Hulugou River Basin in the Qilian Mountains. Global Planet Change, 122, 345-361. https://doi.org/10.1016/j.gloplacha.2014.10.001, 2014a.

Li, Z.X., Qi, F., Wei, L., Tingting, W., Yan, G., Yamin, W., ... & Li, L. : Spatial and temporal trend of potential evapotranspiration and related driving forces in Southwestern China, during 1961–2009. Quater inter, 336, 127-144. https://doi.org/10.1016/j.quaint.2013.12.045, 2014b.

Li, Z.X., Qi, F., Wang, Q. J., Song, Y., Aifang, C., & Jianguo, L. : Contribution from frozen soil meltwater to runoff in an in-land river basin under water scarcity by isotopic tracing in northwestern China. Global Planet Change, 136, 41-51. https://doi.org/10.1016/j.gloplacha.2015.12.002, 2016a.

Li, Z.X., Qi, F., Zongjie, L., Ruifeng, Y., Juan, G., & Yuemin, L. : Climate background, fact and hydrological effect of multiphase water transformation in cold regions of the Western China: A review. Earth-Sci Re, 190,33-57. https://doi.org/10.1016/j.earscirev.2018.12.004, 2018.

Li, Z.X., Qi, F., Wang, Q. J., Song, Y., Jianguo, L., Yongge, L., & Yamin, W. : Quantitative evaluation on the influence from cryosphere meltwater on runoff in an inland river basin of China. Global Planet Change, 143, 189-195. https://doi.org/10.1016/j.gloplacha.2016.06.005, 2016b.

Li, Z.X., Qi, F., Wei, L., Tingting, W., Xiaoyan, G., Zongjie, L., ... & Yaoxaun, S. : The stable isotope evolution in Shiyi glacier system during the ablation period in

the north of Tibetan Plateau, China. Quater inter, 380, 262-271. https://doi.org/10.1016/j.quaint.2015.02.013, 2015.

Li, Z., Yuan, R., Feng, Q., Zhang, B., Lv, Y., Li, Y., ... & Shi, Y. : Climate background, relative rate, and runoff effect of multiphase water transformation in Qilian Mountains, the third pole region. Sci Total Environ, 663, 315-328. https://doi.org/10.1016/j.scitotenv.2019.01.339, 2019.

Li, Z.J., Song, L. L., Jing-zhu, M., & Li, Y. G. : The characteristics changes of pH and EC of atmospheric precipitation and analysis on the source of acid rain in the source area of the Yangtze River from 2010 to 2015. Atmos environ, 156, 61-69. https://doi.org/10.1016/j.atmosenv.2017.02.025, 2017.

Li, Z.J., Zong-Xing, L., Ling-Ling, S., Jin-Zhu, M., & Yong, S. : Environment significance and hydrochemical characteristics of supra-permafrost water in the source region of the Yangtze River. Sci total environ, 644, 1141-1151. https://doi.org/10.1016/j.scitotenv.2018.07.029, 2018.

Liang, E., Shao, X., & Qin, N. : Tree-ring based summer temperature reconstruction for the source region of the Yangtze River on the Tibetan Plateau. Global Planet Change, 61(3-4), 313-320. https://doi.org/10.1016/j.gloplacha.2007.10.008, 2008.

Liu, F., Williams, M. W., & Caine, N. : Source waters and flow paths in an alpine catchment, Colorado Front Range, United States. Water Resour Res, 40(9), 1-17. https://doi.org/10.1029/2004WR003076, 2004.

Lutz, A. F., Immerzeel, W. W., Shrestha, A. B., & Bierkens, M. F. P. : Consistent

908   increase in High Asia's runoff due to increasing glacier melt and precipitation.

909   Nat Clim Change, 4(7), 587. https://doi.org/10.1038/nclimate2237, 2014.

910 Maurya, A. S., Shah, M., Deshpande, R. D., Bhardwaj, R. M., Prasad, A., & Gupta, S.

911   K. : Hydrograph separation and precipitation source identification using stable

912   water isotopes and conductivity: River Ganga at Himalayan foothills. Hydro Pro,

913   25(10), 1521-1530. https://doi.org/10.1002/hyp.7912, 2011.

914 McGuire, A. D., Wirth, C., Apps, M., Beringer, J., Clein, J., Epstein, H., ... & Efremov,

915   D. : Environmental variation, vegetation distribution, carbon dynamics and

916   water/energy exchange at high latitudes. J Veget Sci, 13(3), 301-314.

917   https://doi.org/10.1111/j.1654-1103.2002.tb02055.x, 2002.

918 Mu, Y., Ma, W., Li, G., Niu, F., Liu, Y., & Mao, Y. : Impacts of supra-permafrost

919   water ponding and drainage on a railway embankment in continuous permafrost

920   zone, the interior of the Qinghai-Tibet Plateau. Cold Reg Sci Tech, 154, 23-31.

921   https://doi.org/10.1016/j.coldregions.2018.06.007, 2018.

922 Orlowski, N., Breuer, L., & McDonnell, J. J. : Critical issues with cryogenic

923   extraction of soil water for stable isotope analysis. Ecohydro, 9(1), 1-5.

924   https://doi.org/10.1002/eco.1722, 2016.

925 Pan, X., Yu, Q., You, Y., Chun, K. P., Shi, X., & Li, Y. : Contribution of

926   supra-permafrost discharge to thermokarst lake water balances on the

927   northeastern Qinghai-Tibet Plateau. J Hydro, 555, 621-630.

928   https://doi.org/10.1016/j.jhydrol.2017.10.046, 2017.

929 Peng, T. R., Wang, C. H., Huang, C. C., Fei, L. Y., Chen, C. T. A., & Hwong, J. L. :

Stable isotopic characteristic of Taiwan's precipitation: A case study of western Pacific monsoon region. Earth Planet Sci Let, 289(3-4), 357-366. https://doi.org/10.1016/j.epsl.2009.11.024, 2010.

Prasch, M., Mauser, W., & Weber, M. : Quantifying present and future glacier melt-water contribution to runoff in a central Himalayan river basin. Cryos, 7(3). https://doi:10.5194/tc-7-889-2013, 2013.

Pu, T., He, Y., Zhu, G., Zhang, N., Du, J., & Wang, C. : Characteristics of water stable isotopes and hydrograph separation in Baishui catchment during the wet season in Mt. Yulong region, south western China. Hydro Pro, 27(25), 3641-3648. https://doi.org/10.1002/hyp.9479, 2013.

Pu, J. : Glacier Inventory of China: The Yangtze River Drainage Basin. Lanzhou: Gansu Culture Press, 1-81, 1994.

Qu, J. H., Lu, S. B., Gao, Z. P., Li, W., Li, Z., & Yu, F. : Research on hydrogeochemical characteristics and transformation relationships between surface water and groundwater in the Weihe River. Hydrol Earth sys sc,1-14. https://doi.org/10.5194/hess-2017-654, 2017.

Shi, Y., Niu, F., Lin, Z., & Luo, J. : Freezing/thawing index variations over the circum-Arctic from 1901 to 2015 and the permafrost extent. Sci Total Environ, 660, 1294-1305. https://doi.org/10.1016/j.scitotenv.2019.01.121, 2019.

Uhlenbrook, S., & Hoeg, S. : Quantifying uncertainties in tracer‐based hydrograph separations: a case study for two‐, three‐ and five‐component hydrograph separations in a mountainous catchment. Hydro Pro, 17(2), 431-453. https://doi.org/10.1002/hyp.1134, 2003.

953 Walker, D. A., Jia, G. J., Epstein, H. E., Raynolds, M. K., Chapin Iii, F. S., Copass,

954   C., ... & Nelson, F. ： Vegetation‐soil‐thaw‐depth relationships along a

955   low‐arctic bioclimate gradient, Alaska: Synthesis of information from the

956   ATLAS studies. Perma Peri Pro, 14(2), 103-123. https://doi.org/10.1002/ppp.452,

957   2003.

958 Wang, G., Liu, G., & Liu, L. A. ： Spatial scale effect on seasonal streamflows in

959   permafrost catchments on the Qinghai–Tibet Plateau. Hydro Pro, 26(7), 973-984.

960   https://doi.org/10.1002/hyp.8187, 2012.

961 Wang, G., Hu, H., & Li, T. ： The influence of freeze–thaw cycles of active soil layer

962   on surface runoff in a permafrost watershed. J Hydro, 375(3-4), 438-449.

963   https://doi.org/10.1016/j.jhydrol.2009.06.046, 2009.

964 Wang, G., Tianxu, M., Juan, C., Chunlin, S., & Kewei, H. ： Processes of runoff

965   generation operating during the spring and autumn seasons in a permafrost

966   catchment on semi-arid plateaus. J hydro, 550, 307-317.

967   https://doi.org/10.1016/j.jhydrol.2017.05.020, 2017.

968 Wang, G., Yuanshou, L., Yibo, W., & Qingbo, W. ： Effects of permafrost thawing on

969   vegetation and soil carbon pool losses on the Qinghai–Tibet Plateau, China.

970   Geoderma, 143(1-2), 143-152. https://doi.org/10.1016/j.geoderma.2007.10.023,

971   2008.

972 Wang, T., Wu, T., Wang, P., Li, R., Xie, C., & Zou, D. ： Spatial distribution and

973   changes of permafrost on the Qinghai-Tibet Plateau revealed by statistical

974   models during the period of 1980 to 2010. Sci Total Environ, 650, 661-670.

975   https://doi.org/10.1016/j.scitotenv.2018.08.398, 2019.

976   Wang, X., Chen, R., Liu, G., Yang, Y., Song, Y., Liu, J., ... & Wang, L. : Spatial

977   distributions and temporal variations of the near-surface soil freeze state across

978   China under climate change. Global planet change, 172, 150-158.

979   https://doi.org/10.1016/j.gloplacha.2018.09.016, 2019.

980   West, A. G., February, E. C., & Bowen, G. J. : Spatial analysis of hydrogen and

981   oxygen stable isotopes ("isoscapes") in ground water and tap water across South

982   Africa. J Geochem Explo, 145, 213-222.

983   https://doi.org/10.1016/j.gexplo.2014.06.009, 2014.

984   Wu, Q., Hou, Y., Yun, H., & Liu, Y. : Changes in active-layer thickness and

985   near-surface permafrost between 2002 and 2012 in alpine ecosystems,

986   Qinghai–Xizang (Tibet) Plateau, China. Global Planet Change, 124, 149-155.

987   https://doi.org/10.1016/j.gloplacha.2014.09.002, 2015.

988   Yang, L., Song, X., Zhang, Y., Han, D., Zhang, B., & Long, D. : Characterizing

989   interactions between surface water and groundwater in the Jialu River basin

990   using major ion chemistry and stable isotopes. Hydrol Earth Sys Sc, 16(11),

991   4265-4277. https://doi.org/10.5194/hess-16-4265-2012, 2012.

992   Yang, M., Nelson, F. E., Shiklomanov, N. I., Guo, D., & Wan, G. : Permafrost

993   degradation and its environmental effects on the Tibetan Plateau: A review of

994   recent research. Earth-Sci Re, 103(1-2), 31-44.

995   https://doi.org/10.1016/j.earscirev.2010.07.002, 2010.

996   Yang, Q., Mu, H., Wang, H., Ye, X., Ma, H., & Martín, J. D. : Quantitative evaluation

997   of groundwater recharge and evaporation intensity with stable oxygen and

998   hydrogen isotopes in a semi‑arid region, Northwest China. Hydro pro, 32(9),

999   1130-1136. https://doi.org/10.1002/hyp.11474, 2018.

1000 Yao, Z., Liu, Z., Huang, H., Liu, G., & Wu, S. : Statistical estimation of the impacts of

1001 glaciers and climate change on river runoff in the headwaters of the Yangtze

1002 River. Quater inter, 336, 89-97. https://doi.org/10.1016/j.quaint.2013.04.026,

1003 2014.

1004 Yu, G. A., Liu, L., Li, Z., Li, Y., Huang, H., Brierley, G., ... & Pan, B. : Fluvial

1005 diversity in relation to valley setting in the source region of the Yangtze and

1006 Yellow Rivers. J Geog Sci, 23(5), 817-832.

1007 https://doi.org/10.1007/s11442-013-1046-2, 2013.

1008 Yu, G. A., Brierley, G., Huang, H. Q., Wang, Z., Blue, B., & Ma, Y. : An

1009 environmental gradient of vegetative controls upon channel planform in the

1010 source region of the Yangtze and Yellow Rivers. Catena, 119, 143-153.

1011 https://doi.org/10.1016/j.catena.2014.02.010, 2014.

1012 Zhang, Y., Ohata, T., & Kadota, T. : Land-surface hydrological processes in the

1013 permafrost region of the eastern Tibetan Plateau. J Hydro, 283(1-4), 41-56.

1014 https://doi.org/10.1016/S0022-1694(03)00240-3, 2003.

1015 Zhao, L., Ping, C. L., Yang, D., Cheng, G., Ding, Y., & Liu, S. : Changes of climate

1016 and seasonally frozen ground over the past 30 years in Qinghai–Xizang (Tibetan)

1017 Plateau, China. Global Planet Change, 43(1-2), 19-31.

1018 https://doi.org/10.1016/j.gloplacha.2004.02.003, 2004.

1019 Zhu, X., Wu, T., Zhao, L., Yang, C., Zhang, H., Xie, C., ... & Du, Y. : Exploring the

1020   contribution of precipitation to water within the active layer during the thawing

1021   period in the permafrost regions of central Qinghai-Tibet Plateau by stable

1022   isotopic   tracing.   Sci   Total   Environ,   661,   630-644.

1023   https://doi.org/10.1016/j.scitotenv.2019.01.064, 2019.

1024

1025

1026

1027

1028

1029

1030

1031

1032

1033

1034

1035

1036

1037

1038

1039

1040

Tables:

1042

1043 Table 1 The correlation analysis of $\delta^{18}O$ and d-excess and meteorological factors in

1044 the fixed point (TTH and ZMD) from March,16 to July, 18.

1045

1046

1047

1048

1049

1050

1051

1052

1053

1054

1055

1056

1057

1058

1059

1060

1061

1062

1063

1064

1065

1066

1067

1068

1069

1070

1071 Table 1 The correlation analysis of $\delta^{18}O$ and d-excess and meteorological factors in

1072 the fixed point (TTH and ZMD) from March,16 to July, 18.

	Precipitation (mm)	Temperature (℃)	Ralative humidity (%)	Evaporation (mm)	$\delta^{18}O$(‰)	D-excess (‰)
Precipitation(mm)	1					
Temperature(℃)	0.853**	1				
Ralative humidity(%)	0.760**	0.836**	1			
Evaporation(mm)	0.658**	0.865**	0.586**	1		
$\delta^{18}O$(‰)	-0.518**	-0.671**	-0.555**	-0.636**	1	
D-excess(‰)	0.500**	0.602**	0.524**	0.533**	-0.568**	1

1073 Note: **, Correlation is significant at the 0.01 level (2-tailed).

1074
1075
1076
1077
1078
1079
1080
1081
1082
1083
1084
1085
1086
1087
1088
1089
1090
1091
1092
1093
1094
1095
1096
1097
1098
1099
1100
1101
1102
1103
1104

Figures:

Fig.1 The map of the study area and the sampling point of river water in different ablation period

(Fig.1a was the detail location of the study area in China and Asian and the distribution of fixed point for precipitation, river water and glacier and snow meltwater; Fig.1b was the distribution of sampling point in initial ablation in 2016; Fig.1c was the distribution of sampling point in ablation in 2016; Fig.1d was the distribution of sampling point in end ablation in 2016; Fig.1e was the distribution of sampling point in ablation in 2017; Fig.1f was the distribution of sampling point in ablation in 2018)

Fig.2 Temporal variation of $\delta^{18}O$ and d-excess during the sampling period in study area

(This figure mainly showed the temporal variation of $\delta^{18}O$ and d-excess for different type runoff based on different ablation in 2016 and strong ablation from 2016 to 2018; Fig.2a, b, c showed the change of $\delta^{18}O$ and d-excess in different ablation period for mainstream, glacier and snow runoff and river in permafrost area; Fig.2d, e, f showed the change of $\delta^{18}O$ and d-excess in ablation period from 2016 to 2018 for mainstream, glacier and snow runoff and river in permafrost area)

Fig.3 Spatial variation of $\delta^{18}O$ based on different ablation in 2016 and ablation from 2016 to 2018

Fig.4 Spatial variation of d-excess based on different ablation in 2016 and ablation from 2016 to 2018

Fig.5 The variation of $\delta^{18}O$ and d-excess with the altitude change in study area

(Fig.5a was the variation of $\delta^{18}O$ and d-excess with the altitude change for mainstream; Fig.5b

1127 was the variation of $\delta^{18}O$ and d-excess with the altitude change for river in glacier permafrost

1128 area;Fig.5c was the variation of $\delta^{18}O$ and d-excess with the altitude change for river in permafrost

1129 area; IA in 2016 represents Initial ablation in 2016; A in 2016 represents Ablation in 2016; EA in

1130 2016 represents End ablation in 2016; A in 2017 represents Ablation in 2017; A in 2018

1131 represents Ablation in 2018)

1132 Fig.6 The variation of location evaporation line (LEL) of river water based on

1133 different ablation in 2016 and ablation from 2016 to 2018

1134 Fig.7 The distribution of δD and $\delta^{18}O$ for river water among other water bodies in

1135 study area

1136 (Fig.7a was the plot of $\delta^{18}O$ for river water in different type, supra-permafrost water, glacier snow

1137 meltwater and precipitation; Fig.7b was the plot of δD for river water in different type,

1138 supra-permafrost water, glacier snow meltwater and precipitation; Fig.7c was the plot of δD

1139 versus $\delta^{18}O$ for river water, supra-permafrost water, glacier snow meltwater and precipitation)

1140 Fig.8 Three end element diagram using the mean values of $\delta^{18}O$ and d-excess for river

1141 water in different ablation in 2016 and ablation from 2016 to 2018

1142 Fig.9 Recharge proportion from possible sources to river water in different altitude

1143 during different ablation in 2016 and ablation from 2016 to 2018

1144 Fig.10 Variation of meteorological factors during sampling period

1145   (Shadow represents the ablation period)

1146 Fig.11 Conceptual model map of the recharge form and proportion of the river water

1147 in different ablation period

1148   (Dark green represents the basin of river in permafrost area; Gray and light green represents the

1149   basin of the river in glacier permafrost area)

1150

1151

1152

1153

1154

1155

1156

1157

1158

1159

1160

1161

1162

1163

1164

1165

1166

1167

1168

1169

1170

1171

1172

1173

1174

1175

1176

1177

1178

1179

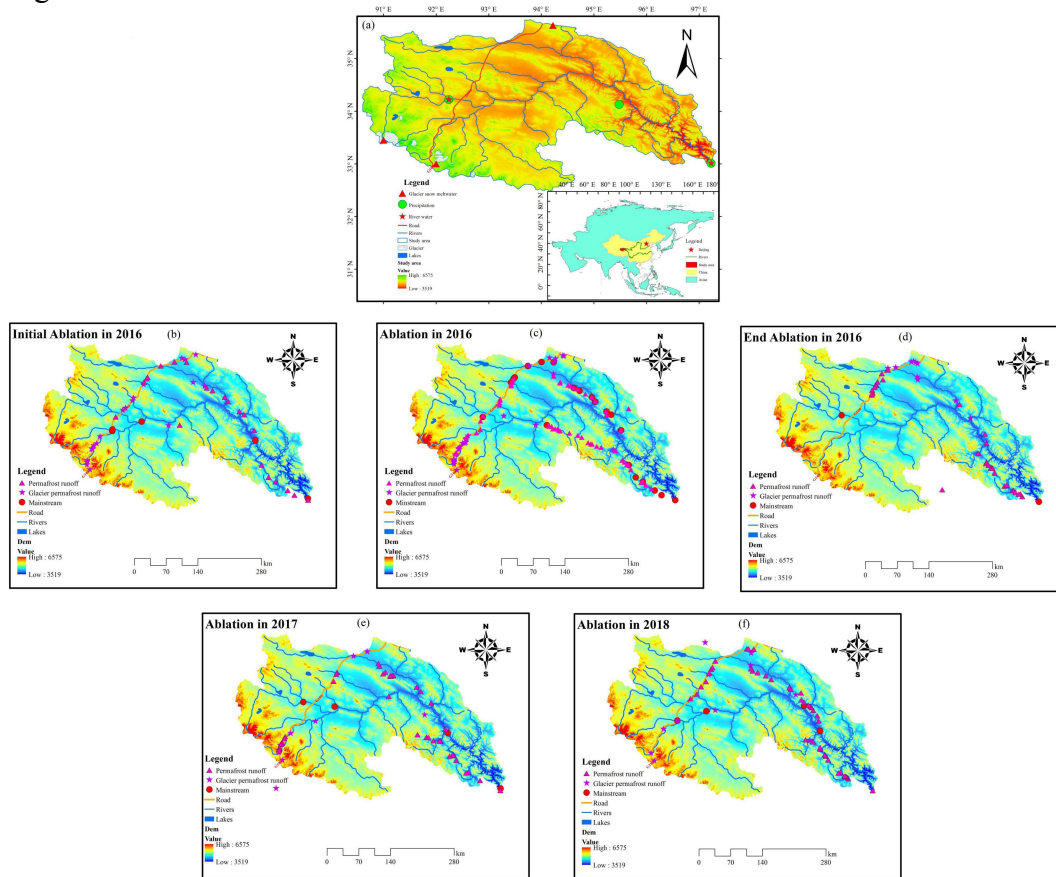1180

1181

1182

1183

1184

1185

1186

1187

1188

1189

1190

1191   Fig.1

1192

1193   Fig.1 The map of the study area and the sampling point of river water in different

1194   ablation period (Fig.1a was the detail location of the study area in China and Asian and the

1195   distribution of fixed point for precipitation, river water and glacier and snow meltwater; Fig.1b

1196   was the distribution of sampling point in initial ablation in 2016; Fig.1c was the distribution of

1197   sampling point in ablation in 2016; Fig.1d was the distribution of sampling point in end ablation in

1198   2016; Fig.1e was the distribution of sampling point in ablation in 2017; Fig.1f was the distribution

1199   of sampling point in ablation in 2018)

1200
1201
1202
1203
1204
1205
1206
1207

1208   Fig.2
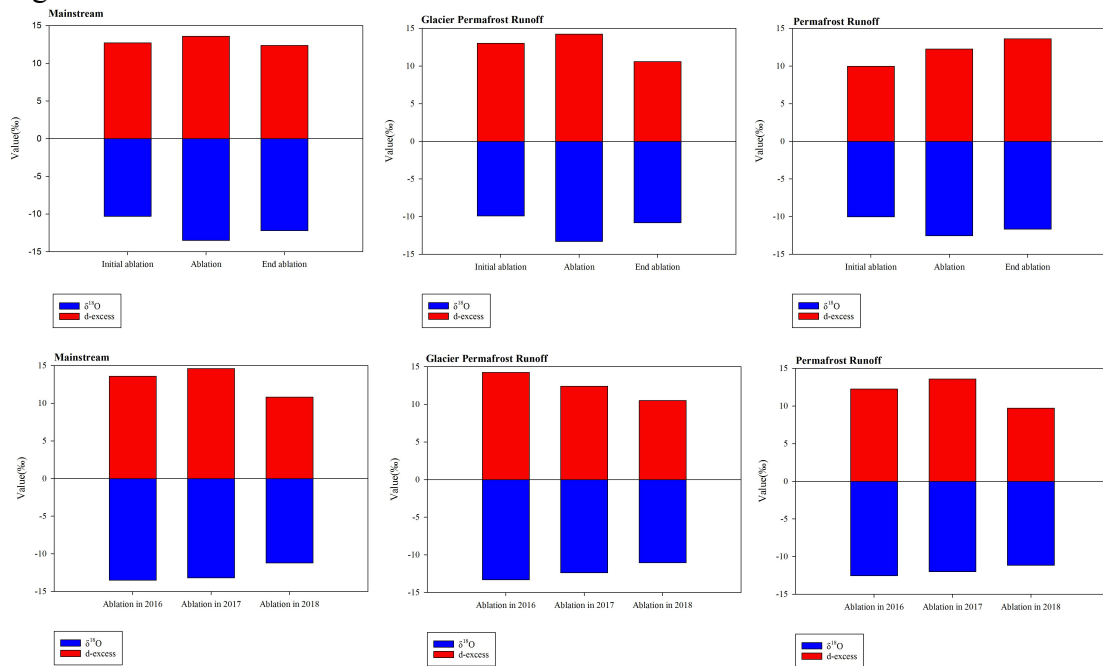
1209

1210   Fig.2 Temporal variation of $\delta^{18}O$ and d-excess during the sampling period in study

1211   area (This figure mainly showed the temporal variation of $\delta^{18}O$ and d-excess for different type

1212   runoff based on different ablation in 2016 and strong ablation from 2016 to 2018; Fig.2a, b, c

1213   showed the change of $\delta^{18}O$ and d-excess in different ablation period for mainstream, glacier and

1214   snow runoff and river in permafrost area; Fig.2d, e, f showed the change of $\delta^{18}O$ and d-excess in

1215   ablation period from 2016 to 2018 for mainstream, glacier and snow runoff and river in permafrost

1216   area)

1217
1218
1219
1220
1221
1222
1223
1224
1225
1226
1227
1228
1229

1230   Fig.3
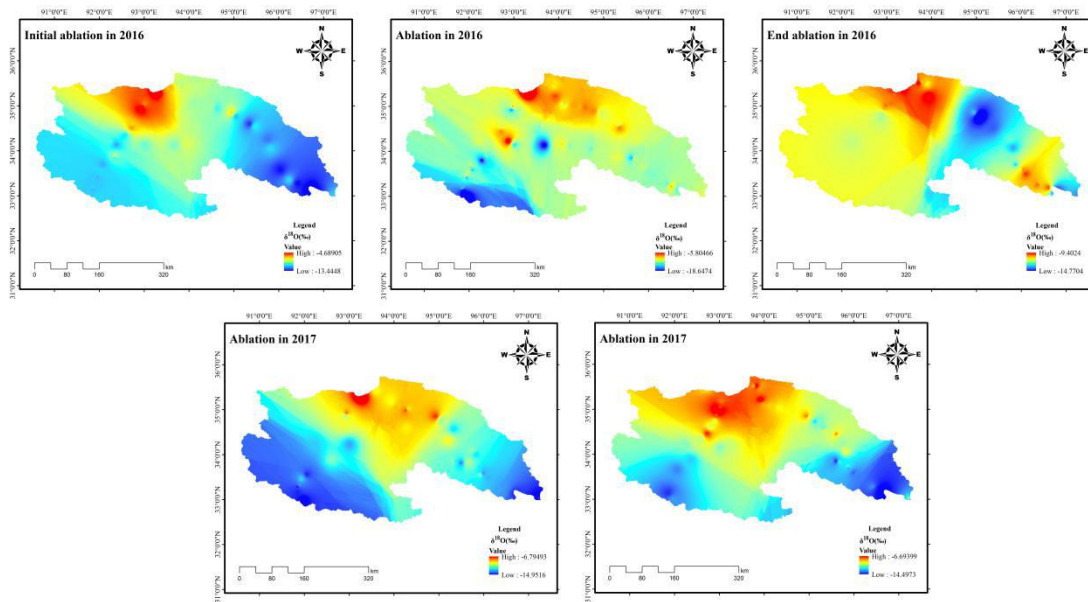
1231

1232   Fig.3 Spatial variation of δ^{18}O based on different ablation in 2016 and ablation from

1233   2016 to 2018

1234
1235
1236
1237
1238
1239
1240
1241
1242
1243
1244
1245
1246
1247
1248
1249
1250
1251
1252
1253
1254
1255
1256
1257

1258   Fig.4
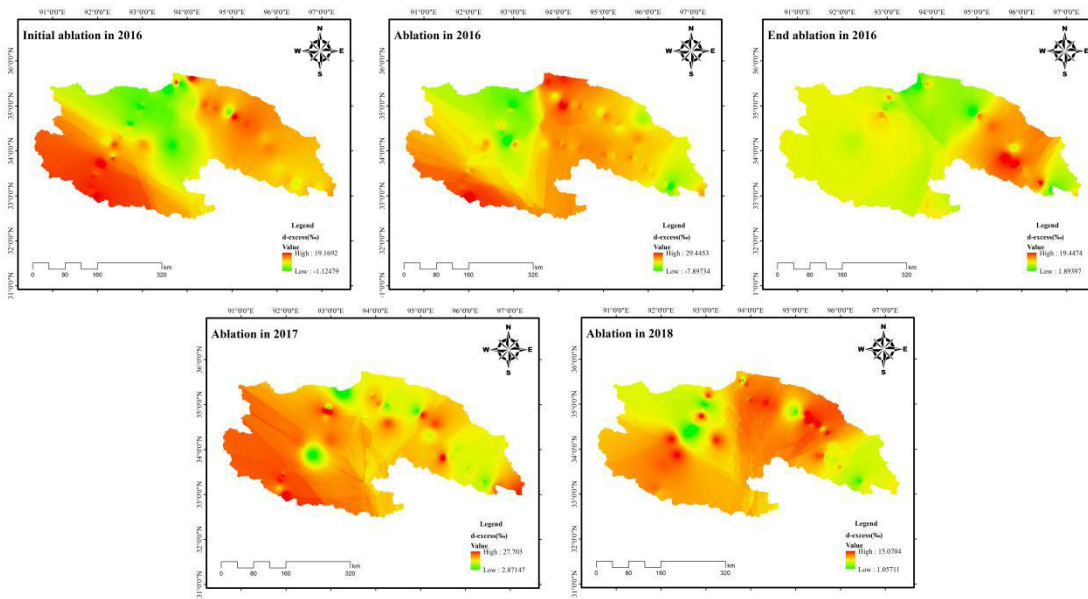
1259

1260   Fig.4 Spatial variation of d-excess based on different ablation in 2016 and ablation

1261   from 2016 to 2018

1262
1263
1264
1265
1266
1267
1268
1269
1270
1271
1272
1273
1274
1275
1276
1277
1278
1279
1280
1281
1282
1283
1284
1285

1286   Fig.5
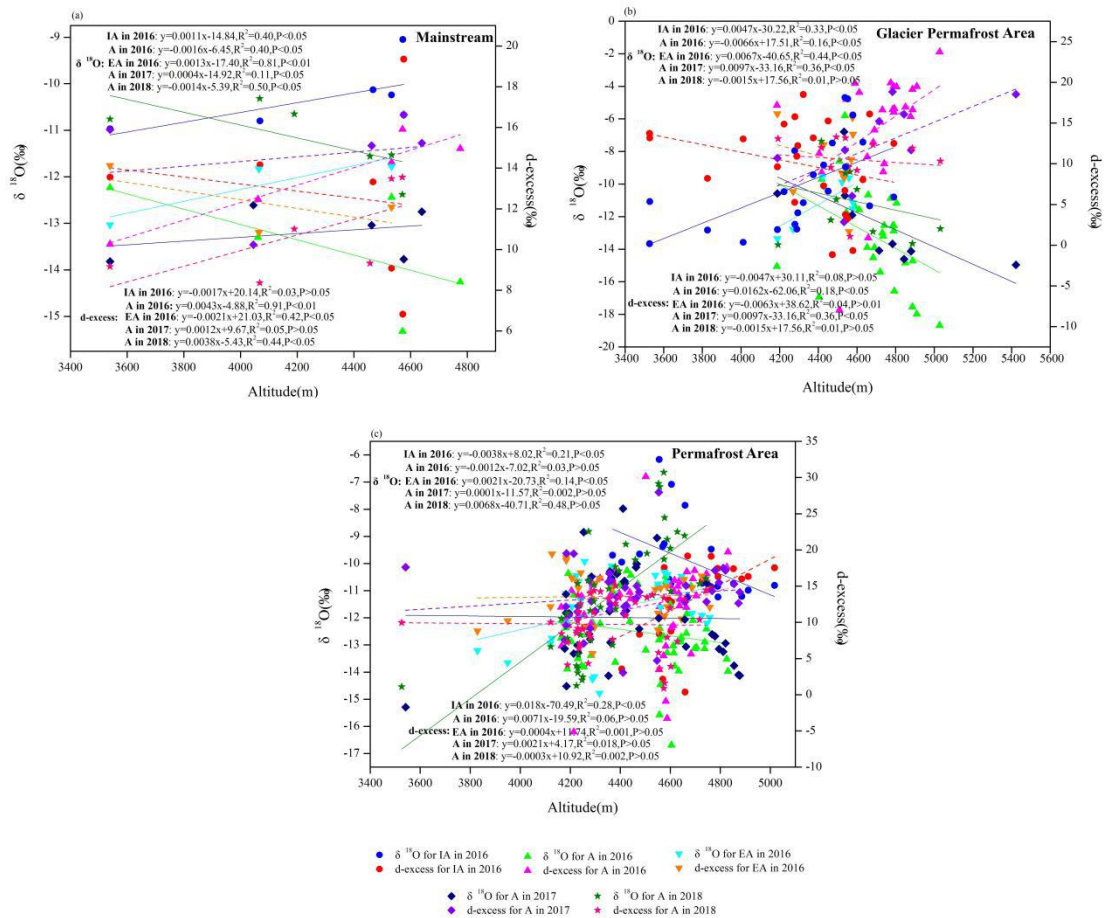
1287

1288   Fig.5 The variation of δ¹⁸O and d-excess with the altitude change in study area

1289   (Fig.5a was the variation of δ¹⁸O and d-excess with the altitude change for mainstream; Fig.5b

1290   was the variation of δ¹⁸O and d-excess with the altitude change for river in glacier permafrost

1291   area;Fig.5c was the variation of δ¹⁸O and d-excess with the altitude change for river in permafrost

1292   area; IA in 2016 represents Initial ablation in 2016; A in 2016 represents Ablation in 2016; EA in

1293   2016 represents End ablation in 2016; A in 2017 represents Ablation in 2017; A in 2018

1294   represents Ablation in 2018)

1295
1296
1297
1298
1299
1300

1301   Fig.6
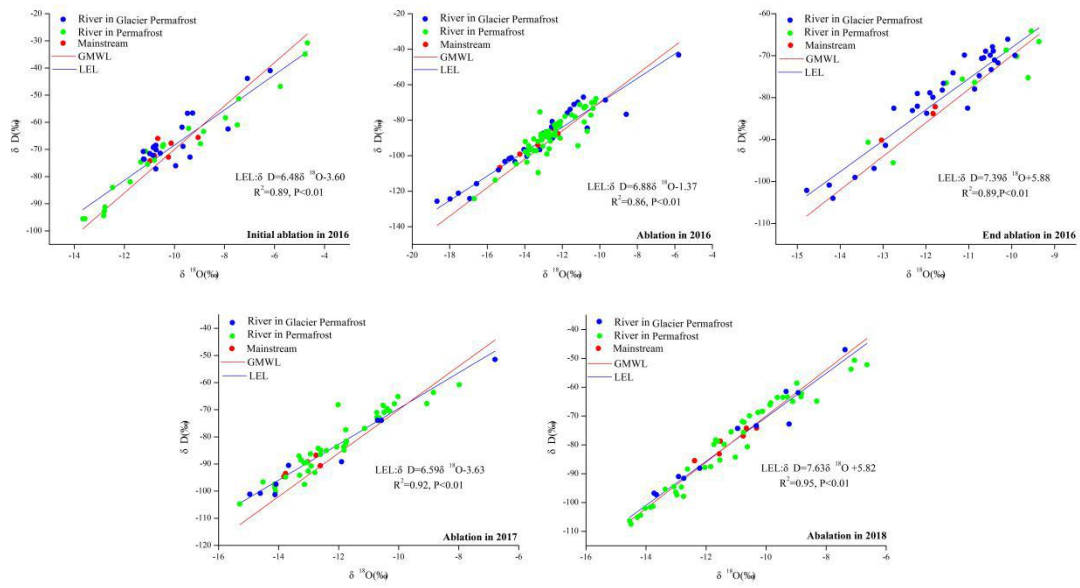
1302

1303   Fig.6 The variation of location evaporation line (LEL) of river water based on

1304   different ablation in 2016 and ablation from 2016 to 2018

1305

1306

1307

1308

1309

1310

1311

1312

1313

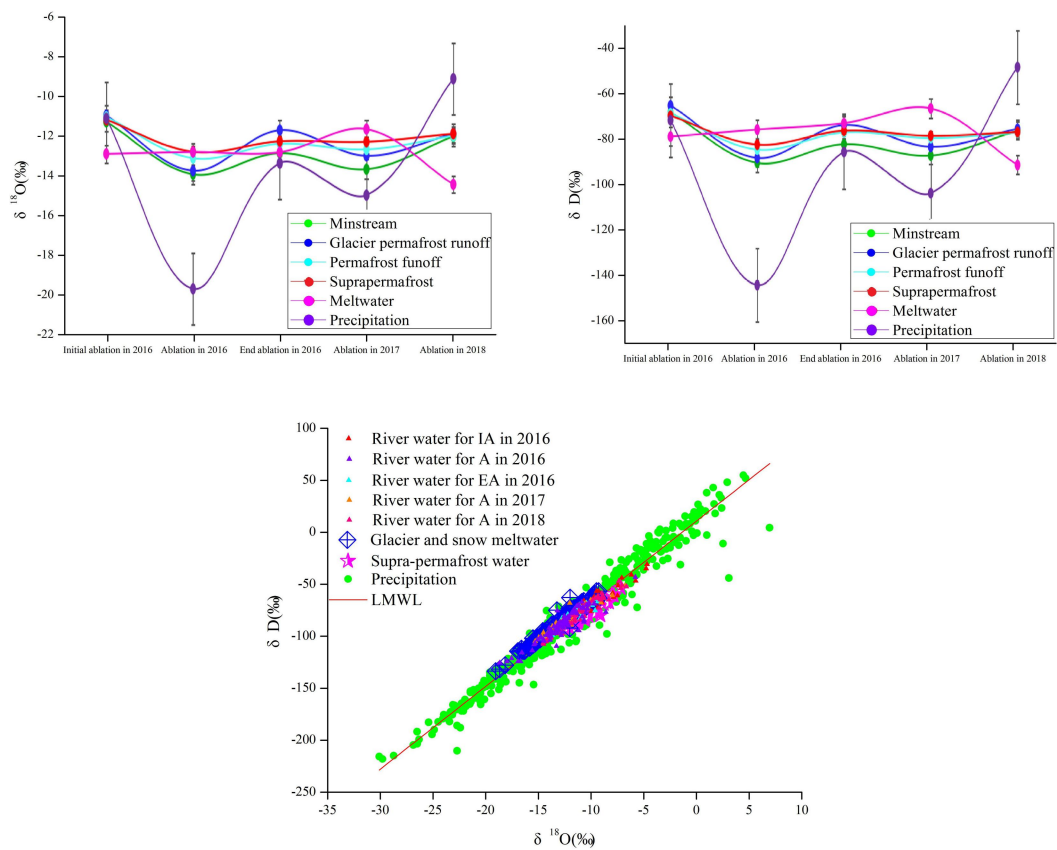1314

1315

1316

1317

1318

1319

1320

1321

1322

1323

1324

1325

1326

1327

1328 Fig.7

1329

1330

1331 Fig.7 The distribution of δD and δ¹⁸O for river water among other water bodies in

1332 study area (Fig.7a was the plot of δ¹⁸O for river water in different type, supra-permafrost water,

1333 glacier snow meltwater and precipitation; Fig.7b was the plot of δD for river water in different

1334 type, supra-permafrost water, glacier snow meltwater and precipitation; Fig.7c was the plot of δD

1335 versus δ¹⁸O for river water, supra-permafrost water, glacier snow meltwater and precipitation)

1336
1337
1338
1339
1340
1341
1342
1343
1344
1345
1346

1347   Fig.8
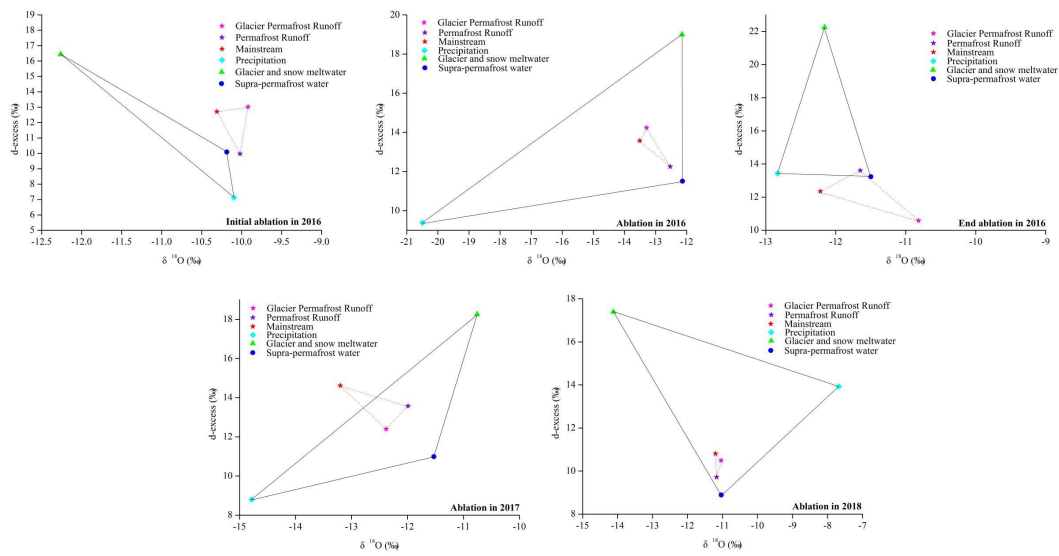
1348

1349   Fig.8 Three end element diagram using the mean values of $\delta^{18}O$ and d-excess for river

1350   water in different ablation in 2016 and ablation from 2016 to 2018

1351
1352
1353
1354
1355
1356
1357
1358
1359
1360
1361
1362
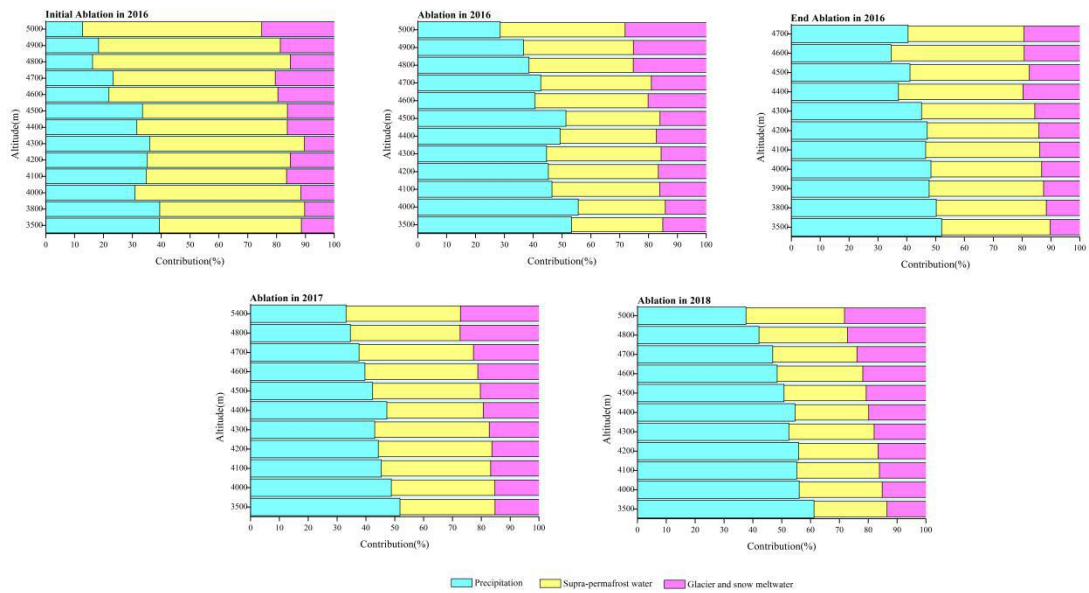1363
1364
1365
1366
1367
1368
1369
1370
1371
1372
1373
1374
1375

1376   Fig.9

1377

1378   Fig.9 Recharge proportion from possible sources to river water in different altitude

1379   during different ablation in 2016 and ablation from 2016 to 2018

1380
1381
1382
1383
1384
1385
1386
1387
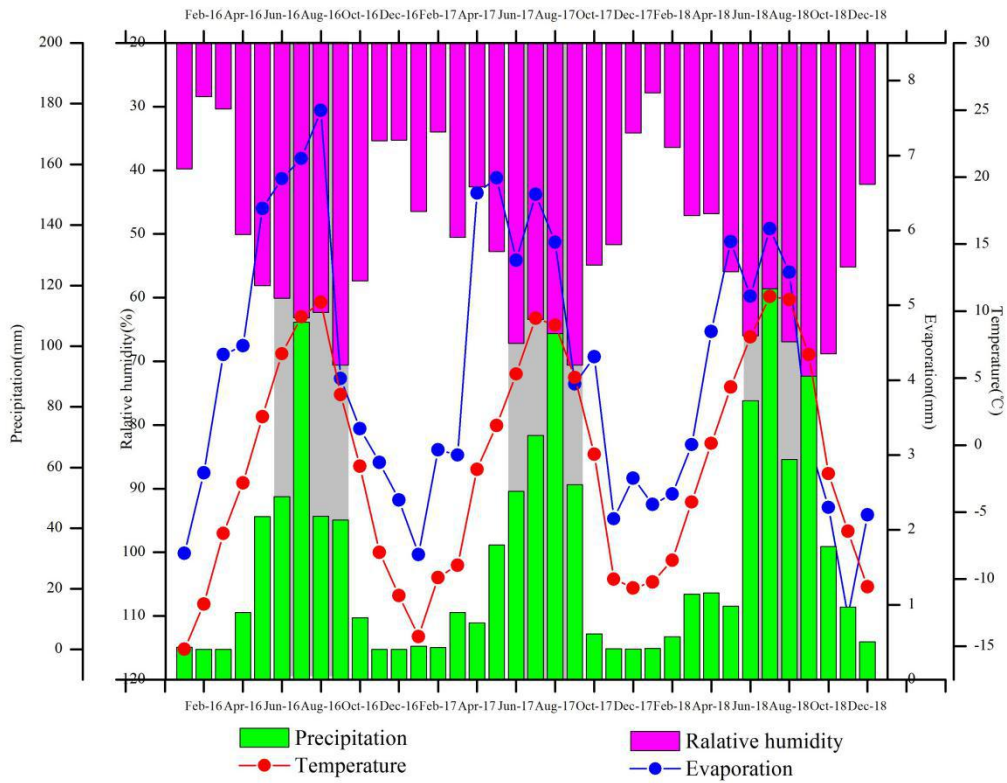1388
1389
1390
1391
1392
1393
1394
1395
1396
1397
1398
1399
1400
1401
1402
1403

1404   Fig.10

1405

1406   Fig.10 Variation of meteorological factors during sampling period (Shadow represents

1407   the ablation period)

1408
1409
1410
1411
1412
1413
1414
1415
1416
1417
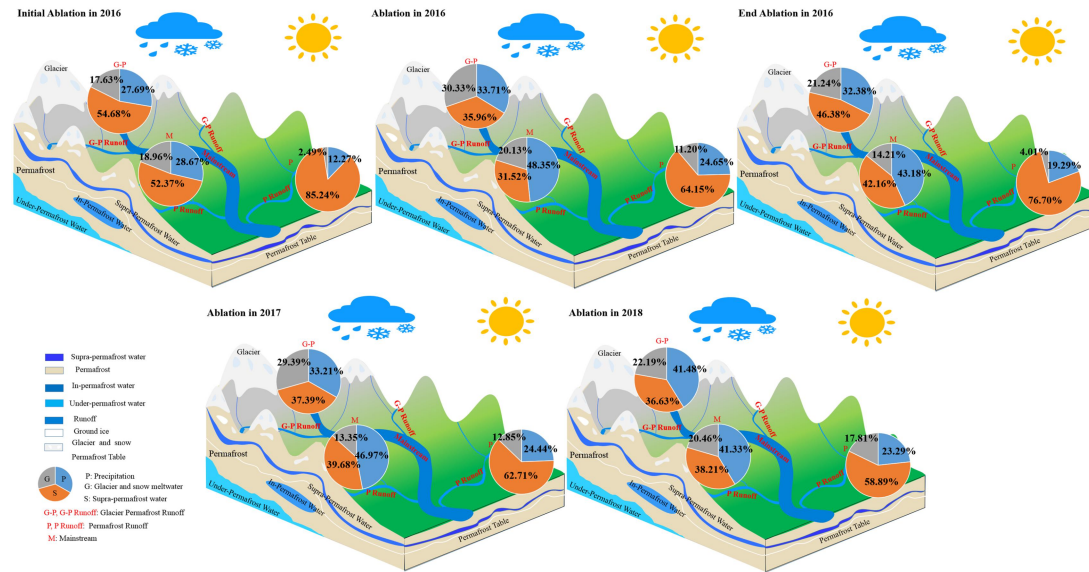1418
1419
1420
1421
1422
1423
1424
1425

1426

1427 Fig.11

1428

1429 Fig.11 Conceptual model map of the recharge form and proportion of the river water

1430 in different ablation period (Dark green represents the basin of river in permafrost area; Gray

1431 and light green represents the basin of the river in glacier permafrost area)